Backward tracking of gas chemistry measurements at Erebus volcano

Alain Burgisser, Clive Oppenheimer, Marina Alletti, Philip R. Kyle, Bruno Scaillet, Michael R. Carroll

Geochemistry Geophysics Geosystems G3

Article
Volume 13, Number 11
22 November 2012
Q11010, doi:10.1029/2012GC004243
ISSN: 1525-2027

Published by AGU and the Geochemical Society

Backward tracking of gas chemistry measurements at Erebus volcano

Alain Burgisser
ISTO, UMR 7327, CNRS/INSU, FR-45071 Orléans, France (alain.burgisser@cnrs-orleans.fr)

ISTO, UMR 7327, Université d'Orléans, FR-45071 Orléans, France

ISTO, UMR 7327, BRGM, FR-45071 Orléans, France

Clive Oppenheimer
ISTO, UMR 7327, CNRS/INSU, FR-45071 Orléans, France

ISTO, UMR 7327, Université d'Orléans, FR-45071 Orléans, France

ISTO, UMR 7327, BRGM, FR-45071 Orléans, France

Institute for Advanced Studies, Le Studium, Orléans, France

Department of Geography, University of Cambridge, Downing Place, Cambridge CB2 3EN, UK

Marina Alletti
ISTO, UMR 7327, CNRS/INSU, FR-45071 Orléans, France

ISTO, UMR 7327, Université d'Orléans, FR-45071 Orléans, France

ISTO, UMR 7327, BRGM, FR-45071 Orléans, France

Philip R. Kyle
Department of Earth and Environmental Science, New Mexico Institute of Mining and Technology, 801 Leroy Place, Socorro, New Mexico 87801, USA

Bruno Scaillet
ISTO, UMR 7327, CNRS/INSU, FR-45071 Orléans, France

ISTO, UMR 7327, Université d'Orléans, FR-45071 Orléans, France

ISTO, UMR 7327, BRGM, FR-45071 Orléans, France

Michael R. Carroll
Department of Earth Sciences, University of Camerino, IT-62302 Camerino, Italy

[1] Erebus volcano in Antarctica offers an exceptional opportunity to probe the dynamics of degassing – its behavior is characterized by an active lava lake through which sporadic Strombolian eruptions occur. Here, we develop a framework for interpreting contrasting degassing signatures measured at high temporal resolution, which integrates physical scenarios of gas/melt separation into a thermodynamic model that includes

new volatile solubility data for Erebus phonolite. In this widely applicable framework, the measured gas compositions are backtracked from surface to depth according to physical templates involving various degrees of separation of gas and melt during ascent. Overall, explosive signatures can be explained by large bubbles (gas slugs) rising slowly in equilibrium from at least 20 bars but at most a few hundred bars in a magmatic column closer to the stagnant end-member than the convecting end-member. The span of explosive signatures can be due to various departure depths and/or slug acceleration below a few tens of bars. Results also reveal that explosive gases last equilibrated at temperatures up to 300°C colder than the lake due to rapid gas expansion just prior to bursting. This picture (individual rise of gas and melt batches from a single, potentially very shallow phonolitic source) offers an alternative to the conclusions of previous work based on a similar data set at Erebus, according to which differences between quiescent and explosive gas signatures are due to the decompression of two deep, volatile-saturated sources that mixed to various degrees (phonolite at 1–3 kbar and basanite at 5–8 kbar).

Components: 14,400 words, 16 figures, 1 table.

Keywords: Erebus volcano; eruptive mechanisms; thermodynamics; volcanic gas.

Index Terms: 8411 Volcanology: Thermodynamics (0766, 1011, 3611); 8428 Volcanology: Explosive volcanism (4302); 8430 Volcanology: Volcanic gases.

Received 21 May 2012; **Revised** 5 October 2012; **Accepted** 8 October 2012; **Published** 22 November 2012.

Burgisser, A., C. Oppenheimer, M. Alletti, P. R. Kyle, B. Scaillet, and M. R. Carroll (2012), Backward tracking of gas chemistry measurements at Erebus volcano, *Geochem. Geophys. Geosyst.*, *13*, Q11010, doi:10.1029/2012GC004243.

1. Introduction

[2] Erebus volcano (Antarctica) is the only presently erupting phonolite volcano [*Kyle et al.*, 1992; *Kelly et al.*, 2008]. It is particularly renowned for its persistent lava lake, the longevity of which implies a bidirectional flow of vesicular and degassed magma within the narrow feeder conduit [*Oppenheimer et al.*, 2009]. The Erebus sustained gas plume, elevation (the crater rim is approximately 3700 m above sea level), and the extremely low atmospheric humidity provide uncommonly favorable circumstances for field spectroscopic measurements of gas emissions from the lava lake [*Oppenheimer and Kyle*, 2008; *Boichu et al.*, 2010, 2011]. Together, Fourier transform infrared and ultraviolet spectroscopic techniques have yielded high temporal resolution measurements of both gas composition and flux. These measurements were able to capture the episodic Strombolian activity that occurs through the lava lake. This behavior, which is shared with that of other well-known volcanoes hosting lava lakes (e.g., Villarrica in Chile [*Witter et al.*, 2004] and Erta Ale in Ethiopia [*Harris et al.*, 2005]), points to the existence of a persistent source of volatiles prone to sudden release. The characterization of such a source, however, is hindered by the complexities that accompany degassing and the evolution of magmas from deep to shallow levels. These include aspects of magmatic differentiation, redox chemistry, and eruptive transitions, which all are caused by the fact that flow instabilities and diffusion processes generate intricate transfers of gas, melt and crystals up and down the conduit.

[3] Among the findings from recent observations are oscillatory variations in gas composition during passive degassing [*Oppenheimer et al.*, 2009] and strongly contrasting gas compositions of explosive versus passive gas emissions [*Oppenheimer et al.*, 2011]. Significantly, the explosively released gas has a much higher ratio of CO_2/CO and a somewhat higher ratio of CO_2/H_2O than the passively emitted gas. This has been interpreted by thermodynamic modeling as evidence for stratified redox conditions within the magmatic system [*Oppenheimer et al.*, 2011], with the differences between quiescent and explosive gas signatures being caused by decompression of two deep, volatile-saturated sources that mixed to varying degrees (phonolite at 1–3 kbar and basanite at 5–8 kbar). Although based on a restricted data set of gas compositions, these conclusions define plausible persistent sources of volatiles.

[4] Our aim here is to develop a different approach for understanding these contrasting degassing signatures by adding a series of physical templates of gas/melt separation during ascent to thermodynamic constraints that include new volatile solubility data

for Erebus phonolite. By assuming that the only melt present in the shallow magmatic system is phonolitic, we test an alternate scenario to that envisioned by *Oppenheimer et al.* [2011] with the aim of completing the possible range of persistent sources of volatiles from which Strombolian explosions arise. Our method is to first calculate under what conditions the measured gas compositions are in thermodynamic equilibrium and then to track these gases backward into the conduit by numerically recompressing and/or reheating them. The common phonolitic source is defined by the pressure domain over which quiescent and explosive gases have the same chemical composition.

2. Observations and Methods

2.1. Activity of Erebus in December 2005

[5] The field observations analyzed here were acquired during the austral summer season from early December 2005 to the beginning of January 2006. During this time, the long-lived lava lake, which is informally referred to as Ray's lake, occupied its usual position in the northeast part of the summit crater (within the so-called Inner Crater). The lake exhibited its typical behavior of continuous convection and degassing [*Giggenbach et al.*, 1973; *Oppenheimer et al.*, 2009]. Superimposed on this characteristic long-term manifestation, however, were sporadic Strombolian explosions resulting from the rupture of gas slugs at the lake surface. In some instances, bubbles of a few tens of meters in diameter distended the entire lake surface a few seconds before explosion. Other explosions, even though of comparable magnitude, were not preceded by visible deformation of the lake surface. The larger events expelled lava bombs up to a few meters in size at speeds of a few tens of meters per second [*Gerst et al.*, 2008]. While most bombs fell within ~200 m of the lake, some were ejected over the crater rim (~200 m vertically above the lava lake) and landed up to 500 m horizontally from the lake. There were typically between one and four such large events, in addition to a similar number of smaller explosions through the lava lake, per day. Included in these observations were small Strombolian explosions at the so-called Active Vent, which is located ~50 m south of the lava lake – during the fieldwork period, lava bombs from these events fell within a few tens of meters of source.

[6] The explosions have been studied using video [e.g., *Dibble et al.*, 2008], seismic [e.g., *Aster et al.*, 2008], radar [*Gerst et al.*, 2008] and infrasound [e.g., *Johnson et al.*, 2008] techniques. Of note, the modeled source centroid for a stack of 293 seismic events that occurred between January 2005 and April 2006 was located ≤400 m beneath the lava lake and somewhat to the west of the lake center [*Aster et al.*, 2008]. Evidence from the directionality of ejecta, however, suggests that the uppermost part of the conduit must be vertical [*Gerst et al.*, 2008]. A remarkable feature of the eruption Very Long Period (VLP) signals are their oscillatory coda, which have durations of a few minutes. The similarity of the VLP signal over thousands of explosions points to a very stable, non-destructive source [*Aster et al.*, 2008; *De Lauro et al.*, 2009]. *Aster et al.* [2008] interpreted these as the result of rapid shallow acceleration of magma within the upper conduit as the lake is refilled.

2.2. Measurement of the Gas Composition

[7] Infrared absorption spectra of the gas discharged from the lava lake were recorded with a MIDAC Corporation Fourier transform infrared (FTIR) spectrometer using the lava lake itself as the infrared source, in the manner reported by *Oppenheimer and Kyle* [2008]. Column amounts of H_2O, CO_2, CO, SO_2, HCl, HF and OCS were retrieved from single beam spectra using a well-tested code [*Burton et al.*, 2000, 2007] that simulates and fits atmospheric transmittance in discrete wave bands (more details in the auxiliary material).[1] Ratios of gas species are obtained by bivariate linear regression of scatterplots (e.g., of CO_2 versus CO or SO_2 versus HCl) of retrieved column amounts spanning a selected time interval. Time series of gas ratios were also charted by dividing the column amounts for pairs of species of interest spectrum-by-spectrum, although in the cases of CO_2 and H_2O, careful corrections were required to subtract first the quantities of these gases present in the ambient air. The volcanic gas species were retrieved in the following spectral regions: 2020–2100 cm^{-1} (CO_2, CO, OCS, H_2O), 2450–2540 cm^{-1} (SO_2), 2690–2830 cm^{-1} (HCl) and 3990–4150 cm^{-1} (HF). Notwithstanding the strong OCS absorption, the 2077 cm^{-1} peak in the CO_2 infrared absorption spectrum provided the most robust retrieval for this species on account of its strength (~1.5×10^{-22} cm $molec^{-1}$). Importantly, we checked for HBr and H_2S but their abundances did not exceed detection limits.

[8] The spectrometer was operated intermittently between 11 December 2005 and 1 January 2006,

[1] Auxiliary materials are available in the HTML. doi:10.1029/2012GC004243.

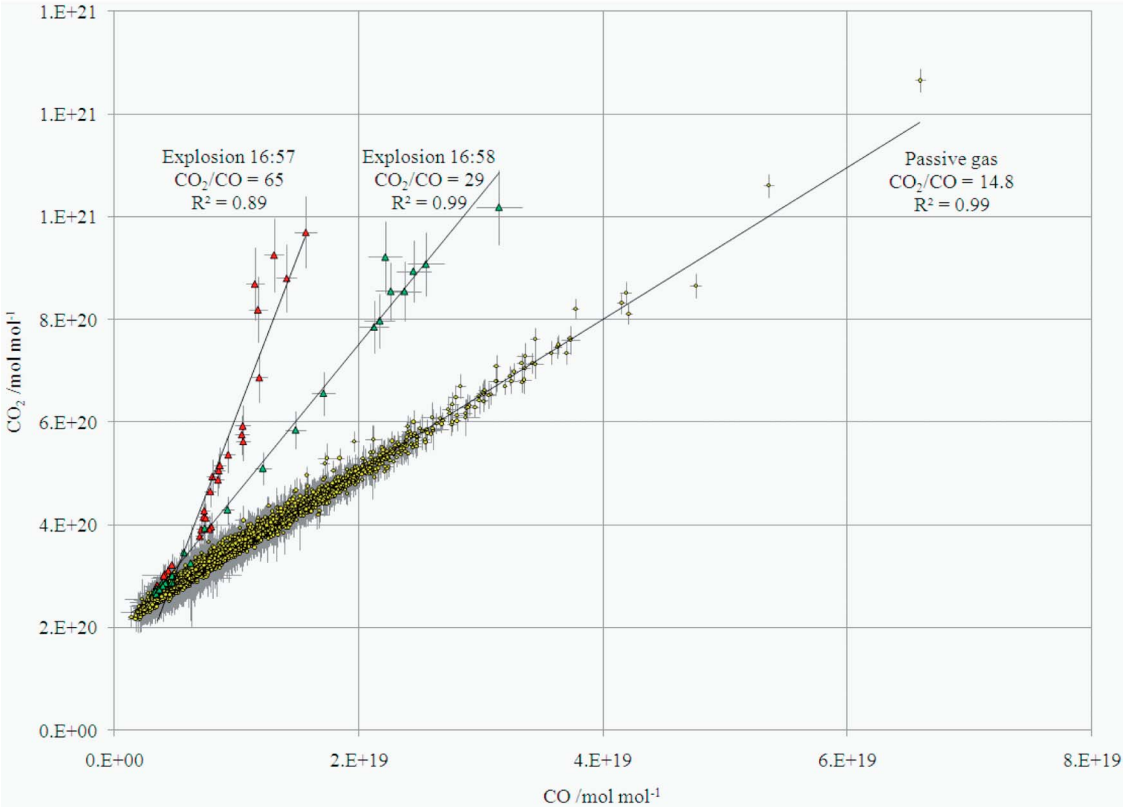

Figure 1. Example of retrieved CO_2 versus CO immediately following a large Strombolian explosion at 16:57 UT on 13 December 2005 (red triangles) and a smaller explosion just over a minute later (green triangles) compared with the signature of passive degassing through the lava lake (yellow circles) over the subsequent 2.5 h. Note the much higher CO_2/CO ratio for the explosively released gas but the differing CO_2/CO ratios of the two explosions.

largely dictated by weather conditions. High quality retrievals of the ratios of SO_2/OCS and CO_2/CO were possible, alongside less precise determinations of the ratios of CO_2/H_2O and CO_2/SO_2. We captured at least 16 Strombolian eruptions through the lava lake, and two explosions sited at the Active Vent. In most cases, the significant quantities of gas released into the crater by the explosions rapidly (within 1–5 s) caused increases in all retrieved gas species but were particularly obvious for CO_2 and OCS. The expelled gases quickly dispersed so that within a minute or so, the gas composition returned to within its typical range for the passive plume emitted from the lava lake.

[9] In order to characterize the composition of the explosively released gas, the first thirty or so data points (i.e., up to 30 s of measurements, depending on burst duration) immediately following each Strombolian eruption were used (Figure 1). Again, bivariate linear regressions were used to evaluate ratios of CO_2/CO, CO_2/H_2O, and so on. Due to the small numbers of data pairs, uncertainties are greater than for the passive gas emission but nevertheless sufficient to resolve differences in explosive gas composition. In Figure 1, two explosions through the lava lake separated by less than 1.5 min in time reveal distinct CO_2/CO ratios. The explosive release of OCS was considerable, dominating the critical wave band (2020–2100 cm^{-1}) in which CO_2, CO and H_2O (as well as OCS) were determined. We thus took great care to ensure validity of the retrievals by comparing results with those obtained for CO, CO_2 and H_2O in alternative regions of the spectrum (spanning other CO_2 absorption features at ~2165 and ~2400–2600 cm^{-1}).

2.3. Thermodynamical Considerations

[10] The oxygen fugacity of magmas plays a crucial role in their thermodynamics via crystal-melt-fluid partitioning, particularly in the case of heterovalent elements such as iron and sulphur. It thereby influences the petrogenesis and physical properties of magmas, and thus the fluid dynamics and style of

volcanic eruptions. What controls oxygen fugacity is less well understood, however. It has recently been proposed [*Giggenbach*, 1996; *Burgisser and Scaillet*, 2007; *Burgisser et al.*, 2008; *Moretti and Baker*, 2008] that magma degassing can drive redox change in an ascending magma, effectively via the interplay of volatile solubility laws and chemical reactions in the gas phase. The main redox reactions governing the chemistry of the gas phase are [*Carmichael and Ghiorso*, 1986; *Moretti and Ottonello*, 2003; *Burgisser and Scaillet*, 2007; *Baker and Moretti*, 2011]:

$$H_2O = H_2 + {}^1/_2O_2 \quad (1)$$

$$H_2S + {}^1/_2O_2 = {}^1/_2S_2 + H_2O \quad (2)$$

$$SO_2 = {}^1/_2S_2 + O_2 \quad (3)$$

$${}^1/_2CO_2 + H_2O = {}^1/_2CH_4 + O_2 \quad (4)$$

$$CO + {}^1/_2O_2 = CO_2 \quad (5)$$

$$OCS + H_2O = CO_2 + H_2S \quad (6)$$

In addition, dissolved sulphur and iron can also affect the redox state of the magma:

$$2FeO_{(melt)} + {}^1/_2O_2 = Fe_2O_{3(melt)} \quad (7)$$

$$FeO_{(melt)} + {}^1/_2S_2 = FeS_{(melt/solid)} + {}^1/_2O_2 \quad (8)$$

All these reactions except (6) involve molecular oxygen; they are diagnostic of and controlling the redox state of the system. Another useful reaction can be built from the relationships (2), (3), (5), and (6):

$$3CO + SO_2 = 2CO_2 + OCS \quad (9)$$

Reactions (1)–(6) enter into our calculations of the equilibrium conditions of the measured gas (temperature, oxygen fugacity, and pressure) and reactions (1)–(7), solubility laws for H_2O, SO_2, H_2S, H_2, CO_2, and mass balance equations allow us to calculate the evolution of the gas composition with increasing pressure according to different degassing scenarios. We describe in the next sections how solubility laws were obtained and the method of solution used by the thermodynamical model.

2.4. Solubility Laws for Erebus Phonolites

[11] Experiments designed to build a water solubility law for Erebus melt composition were performed with an anorthoclase phonolite bomb (ERE13) ejected from the lava lake on December 29, 2005. Experiments were conducted at pressures between 100 and 2500 bars, and at a temperature of 1000°C (conventionally viewed as the temperature of magma in the lava lake). About 50 mg of glass powder from this bomb (see auxiliary material for sample preparation details) was loaded in Au capsules (3 mm outer diameter) together with several deionized water contents (between 2 and 11 wt.%), depending on the experimental pressure. Capsules were crimped, welded shut and stored in a drying oven at 120°C for at least 8 h in order to check for possible leaks. The runs were kept for 84 h in a rapid-quench Internally Heated Pressure Vessel (IHPV), working vertically, pressurized with Ar-H_2 mixtures adjusted to simulate an oxygen fugacity of $\Delta NNO \sim -1.9$ [*Kelly et al.*, 2008]. At the end of each run, capsules were quenched and re-weighed to screen out any charges that had leaked.

[12] Experimental products were all crystal-free glasses, with no more than 10 vol. % bubbles (~40 μm in diameter). Glasses from each run were recovered for analysis. Some glass chips were mounted in epoxy for electron microprobe analysis and other chips were double-face polished for FTIR spectrometry. Major elements were analyzed with a Cameca SX50 electron microprobe using an accelerating voltage of 15 kV, a beam current of 10 nA with a 10-mm defocused beam and counting time of 10 s on the peak and 5 s on the background. Na was always analyzed first in order to minimize loss. Water was analyzed by using a Nicolet 6700 Magna FTIR equipped with a Continuμm optical microscope and a liquid N_2 cooled Mercury Cadmium Telluride detector (MCT/A). Resolution was set at 2 cm^{-1} and a white-light source and CaF_2 beamsplitter were employed to collect data in the spectral range of 2000–8000 cm^{-1}.

[13] Water solubility in our experiments varied between 0.75 wt.% at 100 bars and 7.21 wt.% at 2500 bars (Figure 2a and Table S2 in Text S1 in the auxiliary material). These results are in an excellent agreement with previous studies of *Dunbar et al.* [1994] on Erebus phonolite, and those of *Schmidt and Behrens* [2008] on a Na-phonolite of Montaña Blanca for the same pressure and temperature (Figure 2a). The variation of water solubility with pressure follows a power law. The fugacity of water ($f H_2O$) was then calculated at the run pressure and temperature following *Burnham et al.* [1969], which allowed us to formulate a solubility law of the type:

$$C_i = a_i f_i b_i$$

where C_i is the concentration of the volatile i in weight percent, f_i its fugacity in bar, and a_i and b_i are constants ($a_{H2O} = 0.038$ and $b_{H2O} = 0.677$; Figure 2a). Using two extreme fittings (one based only on the

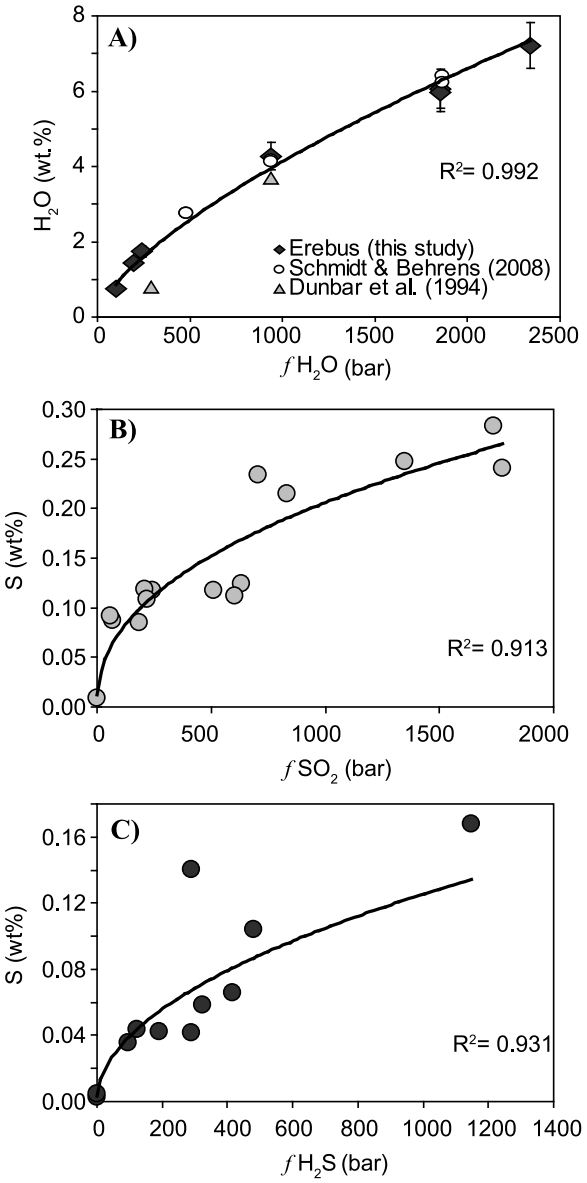

Figure 2. Melt volatile content in phonolites as a function of species fugacity. Curves are average solubility laws with their respective R-squared values. (a) Melt-water content. (b) Sulphur as the oxidized species SO_2. (c) Sulphur as the reduced species H_2S.

experimental melt volatile contents higher than the globally fitted curve, and one based only on the data points lower than the globally fitted curve), errors at 1 kbar are +20% and −10% on melt H_2O content.

[14] We used data for the peralkaline phonolite from Montaña Blanca of *Moncrieff* [1999] to derive a law for the solubility of sulphur (see auxiliary material for detailed method). Experiments were performed in an internally heated pressure vessel at 930°C and between NNO-1 and NNO + 6.5 at 2 kb and at about NNO + 6 at 1.5 kb. The resulting solubilities were fitted by power laws (Figures 2b and 2c), which gave the following constants: a_{SO2} = 0.010, b_{SO2} = 0.437, a_{H2S} = 0.004, b_{H2S} = 0.501. There are, to our knowledge, no other data on sulphur solubility in phonolite that are closer to the Erebus composition and temperature range. This hinders our capacity to quantify the error introduced by applying these regression coefficients to the case of Erebus. The scatter inherent to experimental data has, however, quantifiable consequences on the interpolated melt volatile contents. Interpolation errors at 1 kbar using the same method as in the case of water are +14% and −5% on melt H_2S content, and +3% and −26% on melt SO_2 content. These errors are minimal values for the extrapolation we are carrying out herein.

[15] Carbon dioxide solubility was found by power law regression of the experimental data on the Vesuvius AD 79 "white pumice" phonolite by *Iacono Marziano* [2005]: $a_{CO2} = 5.611 \times 10^{-6}$, b_{CO2} = 1.112. The experiments, in which melts coexisted with a H_2O-CO_2 fluid, were performed at $\log f O_2 \sim$ NNO + 1.3, 1100°C, and 100, 150, and 200 MPa. This temperature is close to that of the Erebus lake, so the extrapolation is mostly compositional. Interpolation errors at 1 kbar using the same method as in the case of water and sulphur are +42% and −3% on melt CO_2 content, which also are minimal values for the extrapolation we are carrying out herein.

2.5. Thermodynamical Model D-Compress

[16] Calculations were done using the model D-Compress of *Burgisser and Scaillet* [2007] and *Burgisser et al.* [2008] with the solubility laws for phonolitic melts described above. Briefly, the model calculates the equilibrium gas composition (H_2O, H_2, O_2, SO_2, H_2S, S_2, CO_2, CO, and CH_4) using reactions (1)–(5) when the pressure, temperature, amount of gas, $f H_2O$, $f H_2$, and $f CO_2$ are fixed. It assumes that the gas is an ideal mixture of non-ideal gases. Since OCS is not among the species calculated by D-Compress (i.e., it does not enter into the mass balance of C, O, and S), it was determined from reaction (6) using the output quantities of CO, SO_2, and CO_2. This procedure induces an error because the additional amount of OCS causes the sum of molar fraction to exceed 100%. This error is small because the typical molar fraction of OCS oscillates between 10^{-7} and 10^{-5}. Renormalization of the other species to include OCS would modify the gas composition by the same amount (i.e. <0.001%), and it

was therefore not attempted in the runs presented here. The equation of state for OCS is valid up to 400 bars, whereas the validity limit of D-Compress is 3 kbar. We framed the possible behavior of OCS at higher pressure by carrying out two extrapolations of OCS density: one using an order three regression of the equation proposed by *Ihmels and Gmehling* [2001], and the other using a constant fugacity coefficient of 1.26, which is the value at 400 bars.

[17] We used the following procedure to constrain the gas equilibrium pressures and temperatures. Discarding HCl and HF, the five remaining measured species are grouped in four ratios: SO_2/OCS, CO_2/CO, CO_2/H_2O, and CO_2/SO_2. For a given $f\,H_2O$, the CO_2/H_2O ratio is used to determine $f\,CO_2$ using the definition of fugacity (e.g., $f_i = \gamma_i\, X_i\, P$, where γ is the fugacity coefficient, X is the gas molar fraction and P is the pressure), and CO_2/CO is used to determine $f\,H_2$ (reactions (1) and (5)). Fitting of each measured gas composition starts by fixing pressure, temperature, and gas content (100% when considering only gas). The $f\,H_2O$ is then adjusted until the desired CO_2/SO_2 is reached, which gives a unique SO_2/OCS value. This operation is iterated at the same temperature but various pressures until the SO_2/OCS value corresponds to that measured. The same procedure is used to determine the equilibrium temperature at a given pressure. The gas composition at equilibrium can thus be equated to any pressure/temperature pair. If, however, any one of H_2, H_2S, CH_4, S_2, or the redox state could have been measured at Erebus, there would be only one possible solution to equilibrate the gas.

[18] The backward tracking, or recompression, of gas and melt starts by calculating the equilibrium composition of all the species assumed to coexist to find the atomic composition of the exsolved volatiles (i.e., amounts of S, O, H, and C). The next step consists in assuming whether the measured gas is in equilibrium with the surrounding melt at the lake surface. If melt is thought to be involved, the total atomic composition of the volatiles (i.e., total volatile content) is found by adding the dissolved volatiles to the gas and taking reaction (7) into account. Compression is always conducted by assuming mass conservation of the volatile elements, either applied to the gas only, or to the mixture of melt and gas. Reversibility of the compression was checked by taking the equilibrium composition of a run at 3 kbar, performing a decompression back to atmospheric pressure and verifying that backward and forward runs were identical. In principle, each gas measurement can be recompressed by this procedure to an arbitrary pressure, provided there is enough gas to start with. The model is calibrated to about 3 kbar, so we stopped all runs that were still saturated in volatiles at that pressure.

2.6. Model Validation and Error Propagation

[19] We quantify in this section the accuracy of determining equilibrium temperatures from gas measurements and of recompressing these gases to high pressures. Errors associated with equilibrium temperatures are assessed thanks to measurements by *Taran et al.* [1995] at Kudryavy volcano. They report gas compositions of high-temperature fumaroles that were established by a combination of gas chromatography and wet chemistry. We use the composition of sample TK1391, which was most likely at equilibrium according to calculations of the thermodynamical model SOLVGAS [*Taran et al.*, 1995]. D-Compress replicates the measured ratios of H_2S/SO_2, CO_2/SO_2, CO_2/CO, and CO_2/H_2O at atmospheric pressure for a temperature of 906°C, which compares well with the 910°C measured by thermocouple and with the 912°C determined by SOLVGAS. We thus consider that D-Compress can estimate equilibrium temperatures to ±5°C.

[20] Errors associated with recompression are estimated by error propagation. Gas-only recompression errors are estimated by taking a gas composition representative of Erebus (median quiescent gas composition, Table 1) and varying the equilibration temperature by ±5°C. As explained above, we use four gas ratios to track gas composition. Relative errors are ±7%, ±1%, <±0.003%, and ±2% for SO_2/OCS, CO_2/CO, CO_2/H_2O, and CO_2/SO_2, respectively. Note that measurement errors are of the same order as these values and that errors due to the numerical resolution are much smaller. The largest source of error for closed system recompressions is linked to melt volatile content. Solubility laws presented above are average values established using all the experimental data (Figure 2). Uncertainties for each dissolved species are estimated by additional laws of maximum melt volatile concentrations that only fit the data above the average curve and, conversely, by minimum laws that only fit the data below the average curve. We carried out three closed-system recompressions starting from the same representative gas composition but using the average, maximum, and minimum solubility laws, respectively. Taking the average law as a reference, Figure 3 presents the relative errors that are induced by the extreme laws on the four gas species ratios used in this study. Overall, errors are <10% at the beginning of the

Table 1. Measured and Calculated Gas Compositions[a]

	Post-Burst Composition, 0.65 bar						Pre-Burst Composition, 1080°C					
	CO_2/CO	CO_2/H_2O	CO_2/SO_2	SO_2/OCS	ΔNNO	T[b] (°C)	CO_2/CO	CO_2/H_2O	CO_2/SO_2	SO_2/OCS	P (bar)	ΔNNO
Explosions[c]												
13/12/05 16:57[e]	*58*	*1.80*	*87*	*27*	−0.79	862	30.7	1.76	58.0	231	1.87	−0.69
13/12/05 23:05	*118*	*0.61*	*50*	*52*	−0.43	795	27.9	0.59	28.7	209	2.69	−0.78
13/12/05 23:09	*34*	*0.14*	*36*	*208*	−1.00	940	21.9	0.14	25.5	647	1.25	−0.99
13/12/05 23:19[d,e]	*87*	*0.94*	*110*	*9*	−0.77	777	17.9	0.90	33.3	40	2.98	−1.16
14/12/05 5:45	*17*	*0.08*	*39*	*331*	−1.34	1028	15.0	0.08	33.1	517	0.82	−1.32
14/12/05 11:45	*30*	*0.07*	*12*	*3500*	−0.78	1054	28.2	0.07	11.9	4341	0.73	−0.77
14/12/05 11:48[e]	*58*	*0.65*	*81*	*14*	−0.94	821	16.4	0.62	28.7	49	2.33	−1.24
15/12/05 3:15[e]	*66*	*1.66*	*160*	*9*	−0.86	812	24.5	1.60	61.6	94	2.44	−0.89
16/12/05 5:51[e]	*97*	*2.59*	*420*	*13*	−0.61	791	58.4	2.55	232.8	949	2.75	−0.14
19/12/05 6:30[e]	*65*	*1.76*	*430*	*17*	−0.80	832	43.1	1.74	233.4	542	2.19	−0.40
19/12/05 9:39[e]	*69*	*1.50*	*65*	*25*	−0.73	838	25.7	1.46	38.8	131	2.12	−0.85
21/12/05 9:38[e]	*128*	*21.0*	*780*	*1*	−0.73	710	71.7	20.15	287.8	833	4.42	0.04
25/12/05 7:53[e]	*93*	*2.35*	*260*	*14*	−0.63	797	48.8	2.31	143.3	592	2.66	−0.29
27/12/05 5:21[d,e]	*103*	*3.99*	*280*	*23*	−0.51	805	72.3	3.94	212.5	1751	2.54	0.05
29/12/05 1:23[e]	*72*	*2.34*	*350*	*5*	−0.88	788	30.3	2.27	105.3	137	2.80	−0.71
31/12/05 6:12[e]	*64*	*1.48*	*400*	*7*	−0.92	805	30.1	1.44	119.9	174	2.54	−0.71
31/12/05 6:36[e]	*57*	*2.96*	*620*	*4*	−1.03	802	32.8	2.88	181.3	176	2.58	−0.64
1/1/06 3:22[e]	*56*	*1.58*	*140*	*18*	−0.86	850	29.4	1.54	77.2	200	1.99	−0.73
Median, 1080°C	60.7	1.00	253	6245	−0.10	1080	29.8[f]	1.57[f]	69.4[f]	220[f]	2.49[f]	−0.72[f]
Median,[d] 829°C	65.5	1.62	150	15	−0.81	829	30.0	1.60	69.0	168	2.50	−0.71
Quiescent degassing												
Top of cycle	*15.5*	*0.30*	*20*	*254*	−1.28	1084						
Bottom of cycle	*14.5*	*0.70*	*45*	*86*	−1.37	1069						
Median,[d] 1080°C	*14.8*	*0.33*	*45*	*188*	−1.33	1080						

[a]All species ratios are molar fractions. Values in italics were measured; other values are model-dependent. See Tables S3 and S4 in Text S1 in the auxiliary material for detailed gas compositions.
[b]Temperatures were calculated to ±1°C.
[c]Explosion times are UTC.
[d]Representative values used in the simulations.
[e]CO_2/CO and CO_2/H_2O ratios are the same as published in *Oppenheimer et al.* [2011].
[f]Median values only, thus not in thermodynamical equilibrium.

recompression and increase with pressure. For simplicity, we take for each species ratio the maximum errors at 1000 bars, which are ±50%, ±10%, ±40%, and ±20% for SO_2/OCS, CO_2/CO, CO_2/H_2O, and CO_2/SO_2, respectively.

3. Physical Templates to Backtrack Volcanic Gases

[21] Combining thermodynamic modeling with physical aspects of gas/melt separation drove us to define simple templates of the Erebus plumbing system. During passive degassing, the role of the melt surrounding the gas is taken into account by two end-member scenarios. One scenario assumes bi-directional flow where gas and melt rise together as a closed system to reach an arbitrarily fixed porosity at the surface. This end-member approaches the behavior of a slowly convecting magma column. The other end-member assumes that the

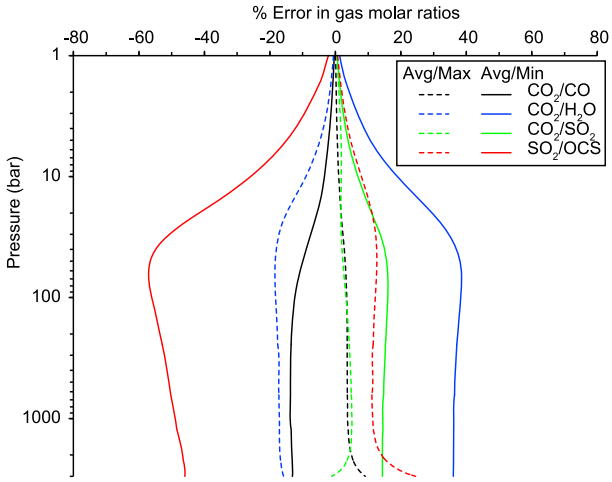

Figure 3. Uncertainties on selected gas species ratios for a typical closed-system compression run. The starting gas composition is the median quiescent gas (Table 1) with 0.0045 wt% initial gas. Errors are given relative to a standard run using average solubility laws.

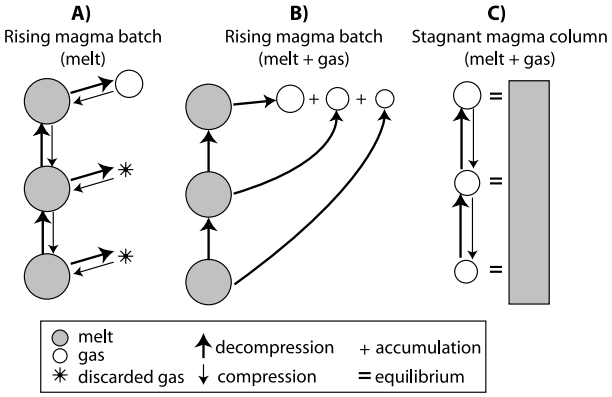

Figure 4. Three open system degassing scenarios. (a) Rising magma batch that loses its gas phase at each pressure step (Rayleigh distillation). (b) Rising magma batch, the gas of which separates at each pressure step, accumulates separately from the melt during ascent and equilibrates at atmospheric pressure. (c) Stagnant magma column that loses its gas all along its depth but that is in equilibrium with it at all depths. Note that the evolution of the melt volatile content with pressure of this scenario is similar to that of the complete mixing scenario of *Witham* [2011].

gas rises independently from any point within the otherwise still magma column. This case, clearly an extreme explanation of the passive degassing at Erebus, frames the range of possible convection patterns by simulating a stagnant melt column undergoing steady degassing. Explosions, on the other hand, are triggered by visible, large (metric to decametric) gas bubbles breaking through the lake surface. The behavior of these large bubbles, conventionally referred to as gas slugs, is also framed by simplified scenarios. The first end-member assumes that gas and melt rise together in closed system to reach a high, arbitrary porosity at the surface. This represents a slug moving slowly enough to maintain chemical equilibrium with a thin melt shell. The other end-member considers a fast-rising slug that moves independently from the melt.

[22] The procedure we use to simulate quiescent degassing differs from the open-system (with respect to the melt) degassing that other models use [*Newman and Lowenstern*, 2002; *Papale*, 1999; *Papale et al.*, 2006; *Oppenheimer et al.*, 2011]. Usually, runs are carried out by decompressing melt and gas to lower pressure in small increments, and the gas is discarded (reset to zero) before the next iteration is performed (Figure 4a). Since D-Compress is based on the presence of gas, such resetting is not possible. Instead, decompression is simulated by removing an aliquot of gas so that a small but finite amount (between 0.1 and 0.001 wt%) of gas remains for the next iteration [*Burgisser et al.*, 2008]. This procedure approaches a Rayleigh distillation and is valid only when a small length of the conduit is taken into account because it simulates the rise of a magma batch while letting the gas leak freely out of the batch. This procedure yields the evolution of melt volatile content as a function of pressure, and a single gas composition at the last step of decompression (Figure 4a). When studying the behavior of the gas, however, one has to consider the fate of the gas aliquots that are discarded at each pressure step. There are several ways to do so. By definition, each aliquot rises independently and re-equilibrates at atmospheric pressure because the gas motion is perfectly decoupled from the rising melt. This generates an array of compositions, one for each possible originating pressure along the conduit. The gas measured at the surface will thus be the result of the accumulation of each aliquot, the composition of which can be calculated by adding the aliquots at each pressure step (Figure 4b). This procedure, however, overlooks the fact that the gas aliquots are likely to interact with the melt they encounter while rising, ultimately equilibrating with it. The alternative view we adopted is to consider a stagnant melt column undergoing steady degassing. In this view, the gas rises independently from any point within the column, only encountering melt that is in equilibrium with it. This situation is modeled by first decompressing the gas on its own, which yields fugacity values for each gas species as a function of total pressure. The melt volatile content of each soluble species is then recalculated at all pressures using species fugacities and the corresponding solubility laws (Figure 4c).

[23] Figure 5 shows an example of decompression according to these three open-system degassing scenarios. The starting pressure was set to 3 kbar (a value ensuring volatile saturation) with a gas composition in equilibrium with the average volatile content of phonolite-hosted melt inclusions (0.14 wt% H_2O, 846 ppm CO_2, and 530 ppm S) [*Oppenheimer et al.*, 2011]. We distinguished the respective contributions of atmospheric equilibration and accumulation of the gas aliquots. The gas aliquot emitted by the rising batch at, say, 1 kbar has a CO_2/CO ratio of 36. If the melt batch stops rising, the gas composition at that pressure is equal to the sum of all the aliquots up to that point, which yields a CO_2/CO of 22 (blue arrow in Figure 5a). If this gas reaches the vent without further interactions, CO_2/CO decreases to 10 (red arrow in Figure 5a). This illustrates that re-equilibration to atmospheric pressure is crucial when evaluating the effect of

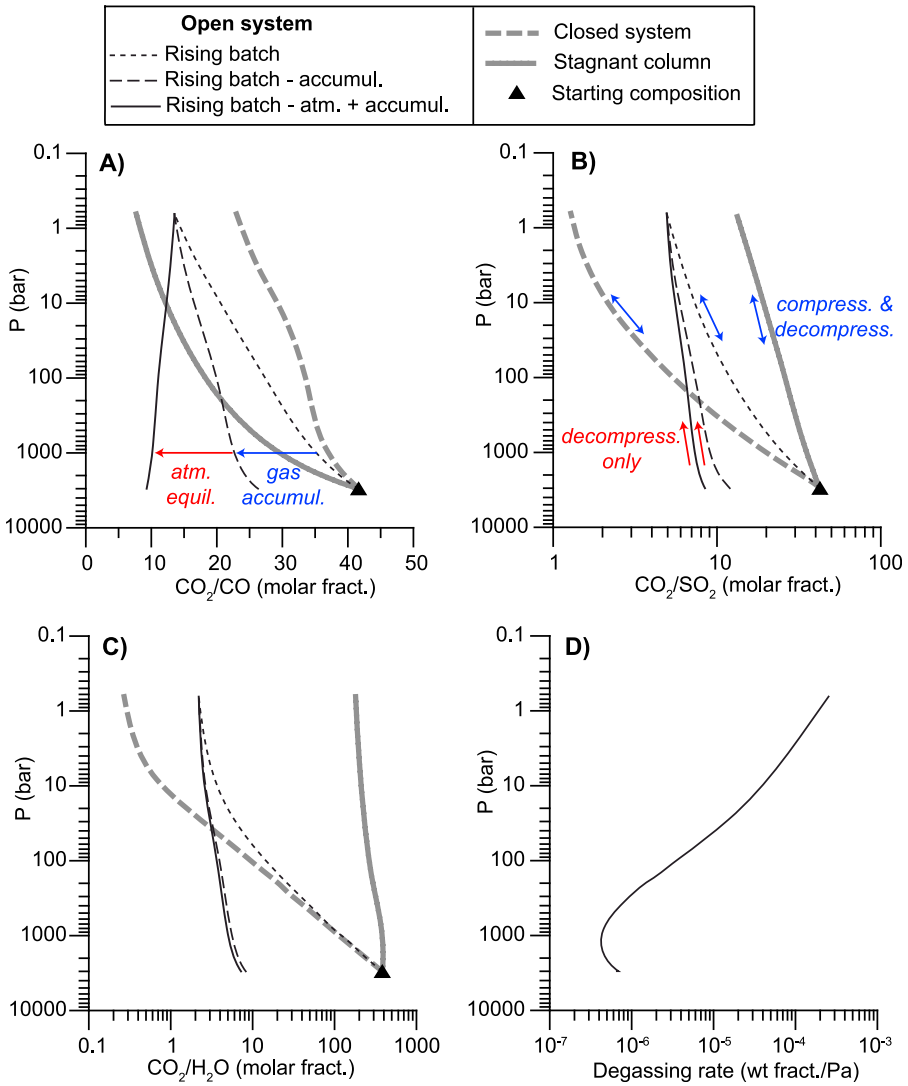

Figure 5. Evolution of gas composition and degassing rate as a function of pressure for decompression runs representing different degassing scenarios. (a–c) Gas composition as measured by species ratios. "Rising batch" corresponds to the scenario depicted in Figure 4a, and "Rising batch – atm. + accumul." corresponds to that depicted in Figure 4b. For reference, stagnant and convecting column runs are shown in gray and the starting gas composition is represented by a black triangle. Arrows in Figure 5a indicate the respective effects of atmospheric equilibration (red) and gas accumulation (blue) during ascent. Arrows in Figure 5b indicate whether runs can be achieved by compression only (red) or by both compression and decompression (blue). (d) Degassing rate.

stalling of a melt batch, but hardly affects the final gas composition at the vent if the batch reaches the surface. This is because degassing rate is highest at low pressure (Figure 5d).

[24] Compression runs of the open-system degassing of a steadily rising magma batch (Figure 4b) cannot be conceived in the same way as decompression runs because the contribution of each atmospherically equilibrated gas aliquot to the gas composition measured at the vent is unknown. As a result, the amount of gas that needs to be reintroduced in the system at each pressure step is unknown (i.e., accumulation cannot be backtracked). The case of a magma batch rising steadily from high pressure to the surface (Figure 4a), however, can be backtracked. Figure 5 shows that its behavior is intermediate between that of a stagnant (Figure 4c) and a convecting column (closed system degassing). In order to maximize the span of backtracked compositions, we decided to keep in our analysis these two last scenarios and leave the case of a steadily rising magma batch aside. As mentioned earlier, both end-members are extreme explanations of the passive degassing; the closed

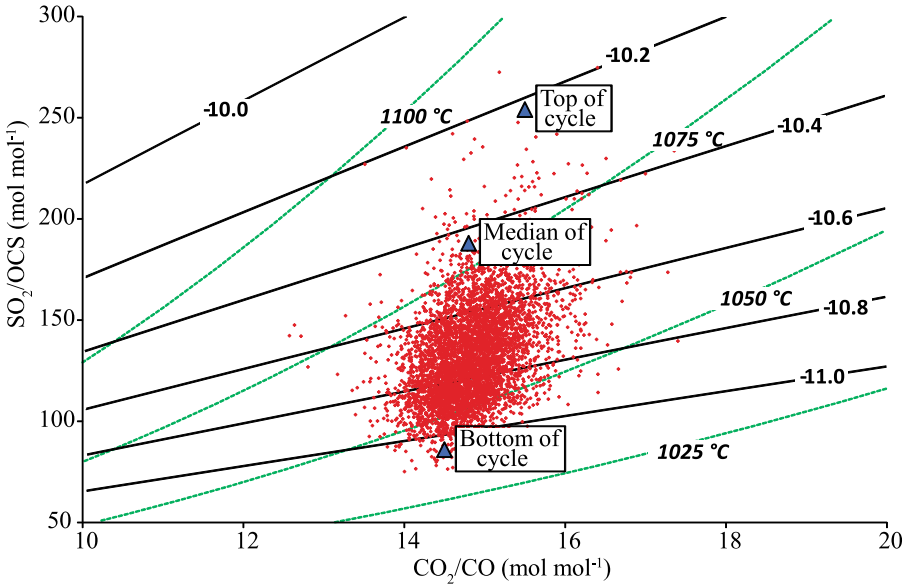

Figure 6. SO_2/OCS versus CO_2/CO for ~5000 spectra representing passive degassing from the lava lake on 15 December 2005. These are superimposed on curves computed for the equilibria in reactions (5) and (9) for X_{CO} = 0.016 and atmospheric pressure (0.65 bar). Steeper curves are for constant temperature (indicated in Celsius) and the flatter curves are for constant f O_2 (shown in units of $\log_{10}$(bar)). The three labeled points are high, low, and median representative compositions.

system run because the lake surface is in reality permeable to gas, and the open system because of the field evidence that the melt column is visibly not stagnant. Our general feeling is that further distinctions between the different degassing scenarios would necessitate a much finer treatment of the dynamics of gas bubbles and melt motion within the lava lake and its feeder system.

4. Results on Equilibrium Conditions

[25] We used the molar ratios of SO_2/OCS, CO_2/CO, CO_2/H_2O and CO_2/SO_2 retrieved by FTIR spectroscopy to establish the temperature, pressure, and redox state of the gas. We first focus on measures made during quiescent degassing of the lava lake because this ensures that the measured gas was at atmospheric pressure (~0.65 bar at the lava lake surface). We then explore the conditions prevailing during explosions.

[26] Figure 6 shows a selection of the two best constrained ratios, SO_2/OCS and CO_2/CO, from spectra collected on 15 December 2005, during quiescent degassing of the lake. Superimposed on the plot are curves for SO_2/OCS and CO_2/CO calculated at thermodynamic equilibrium and atmospheric pressure for a range of oxygen fugacity and temperature, based on reactions (5) and (9) and X_{CO} = 0.016. The X_{CO} value was obtained by assuming that the gas is only composed of five species (SO_2, OCS, CO_2, CO, and H_2O) and by using the average values of the four respective ratios (Table 1). Although a coarse assumption, fixing X_{CO} yields a synoptic view of the temperature and redox ranges of the quiescent gas: at constant oxidation state, a decrease in temperature causes both ratios to rise. The locus of the median value for the 2005/2006 field season shown in Figure 6 suggests that the lava lake temperature is ~1080°C and f O_2 is $\sim 10^{-10.4}$ bar (ΔNNO = −1.33). The spread of values in Figure 6 is due to regular (~10 min) upwellings within the lake, which cause small scale oscillations of the gas composition (Figure 7) [*Oppenheimer et al.*, 2009].

[27] A determination that takes into account the two other ratios (CO_2/H_2O and CO_2/SO_2) and thus that releases the need of assuming a fixed X_{CO} was made with our thermodynamical model on the two extreme compositions shown in Figure 6. One end-member composition corresponds to the gas at the lowest part of the flux cycle, and the other corresponds to the highest part of the cycle (Table 1). At atmospheric pressure, these compositions equilibrated at 1069°C and 1084°C, respectively, with $f O_2$ of $10^{-10.6}$ bar (ΔNNO = −1.28) and $10^{-10.3}$ bar (ΔNNO = −1.37). These values are distinct when taking into account model uncertainty (±5°C), which suggests that chemical oscillations are linked to

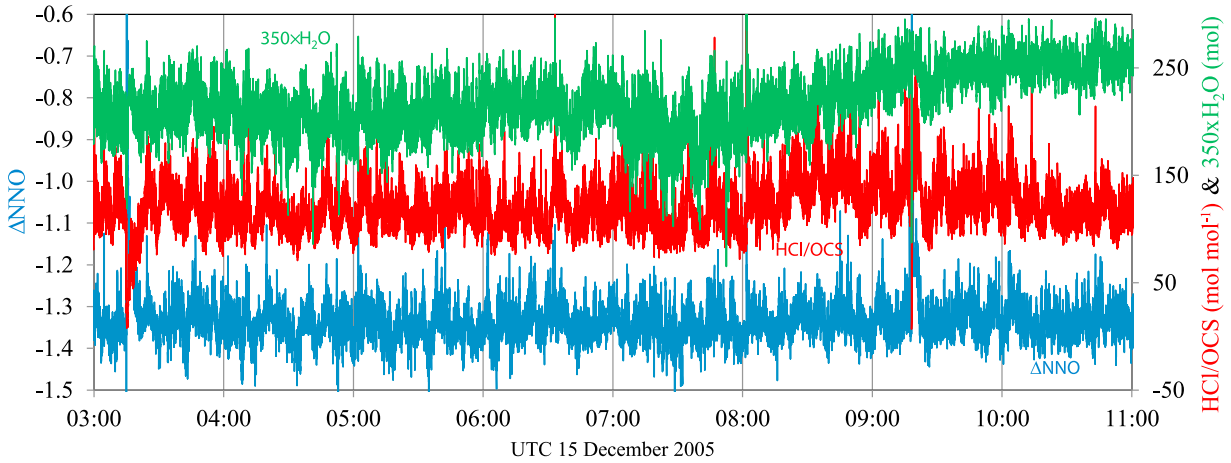

Figure 7. Eight hours on 15 December 2005 of the 1 Hz-recorded molar ratio of HCl/OCS in the gas plume emitted from the lava lake (in red), ΔNNO in log (bar) (in blue), and the mole fraction of water in the gas plume (in green). The ΔNNO is computed from the observed CO_2/CO ratio at 1080°C. The HCl/OCS time series most clearly indicates a ~10 min period oscillatory behavior of the lava lake associated with the pulsed input of magma from the conduit (which is at its peak when HCl/OCS is high). The correspondence between HCl/OCS and ΔNNO fluctuations is generally clear, indicating that the magma pulses entering the lake are about 0.1 log units more oxidized than the lava lake itself. The X_{H2O} oscillations are also phase-locked with those exhibited by HCl/OCS and ΔNNO, indicating that the magma pulses entering the lake are strongly degassing water at low pressure. Of note are two explosions, one at 06:15 UT, the other at 09:19, which are marked by instantaneous decrease in HCl/OCS and increase in $f\,O_2$.

temperature oscillations. These values also bracket 1080°C, which we use as the most probable lake temperature. We thus selected a representative average gas composition that is in equilibrium with that temperature at atmospheric pressure (Figure 6 and Table 1).

[28] The Strombolian explosions have species ratios distinct from the quiescent degassing values. In particular, the SO_2/OCS ratios are smaller (3–25) and the CO_2/CO ratios are higher (50–100) than their quiescent counterparts (Table 1). The CO/CO_2 and SO_2/OCS ratios of individual explosions are sufficiently well characterized (e.g., Figure 1) that we are convinced this spread of values is real. This could be caused by changes in either pressure, or temperature.

[29] As a starting point, we consider whether the data may be explained by a large isothermal decrease in pressure. Assuming for now that the ascending slug was fast enough to freeze chemical reactions and preserve the gas composition at depth allows us to fix temperature to that of the lake. Using the four measured ratios and fixing 1080°C for the magma temperature, it is possible for D-Compress to calculate the equilibrium pressure for each of the 18 explosions of Table 1. Figure 8a shows that the equilibration pressures range from 1.2 to >3000 bars. Not only most equivalent depths (4 m to >10 km) substantially exceed the seismic source depth of less than 400 m, but it is also doubtful that the gas slugs would have been rising from such depths fast enough to quench the gas composition. High temperature, high pressure gas kinetics involving magmatic species are not known precisely, but it can safely be assumed that they keep pace with slug ascent from such depths. For instance, the conversion of CO into CO_2 via reaction (5) takes place on a timescale of order 8×10^{-2} s at 1080°C and 10 bars (G. P. Smith et al., GRI-Mech 3.0, 2011, available at http://www.me.berkeley.edu/gri_mech/). The same reaction taking more than 1 s below 780°C, quenching of the gas is most likely to occur upon cooling at atmospheric pressure.

[30] An alternative process would be a more realistic adiabatic (isentropic) expansion of the gas bubble, accompanied by cooling and immediate re-equilibration. That the gas is able to remain in thermodynamical equilibrium at all times is supported by the fact that high temperature gas kinetics is faster than slug ascent. Gas temperature can thus be calculated by fixing pressure to the atmospheric value. Figure 8b shows that equilibration temperatures at 0.65 bar range from 700 to 1050°C. To first order, this span is reasonable because the larger values are never higher than those of the quiescent degassing, and a 300°C cooling when the slug bursts at the surface is conceivable.

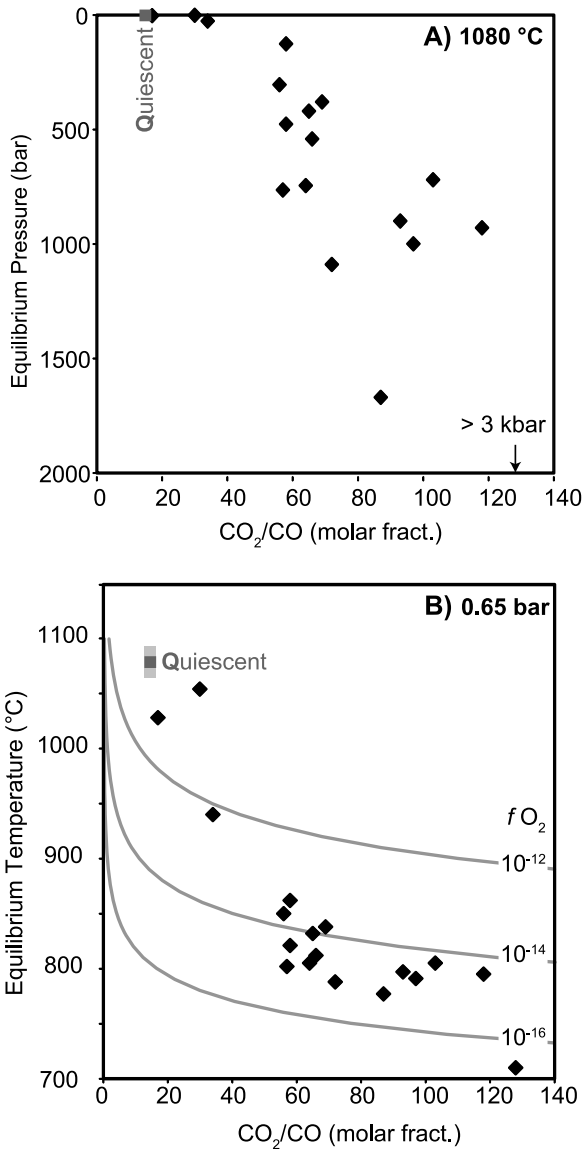

Figure 8. Equilibrium pressures and temperatures of 18 explosions measured in December 2005 as a function of CO_2/CO. (a) Equilibrium pressures at a constant temperature of 1080°C. This assumes that chemical reactions were slow enough to preserve the gas composition at depth despite slug ascent and decompression. The dark gray point marks the median value for quiescent degassing. Note that one explosion would equilibrate at a pressure higher than the validity limit of the model. (b) Equilibrium temperatures at a constant atmospheric pressure. This assumes that chemical reactions were fast enough to keep pace with ascent-driven decompression. The dark gray point marks the median value for quiescent degassing and the light gray area spans the full range of calculated temperatures. Grey curves mark constant oxygen fugacity values and illustrate how the CO_2/CO ratio varies with temperature.

[31] Details of gas bubble explosion are beyond the scope of this work, but important insights can be drawn from an idealized case. If, when the slug reaches the lake surface, skin expansion just before or at rupture is fast enough to prevent dissipative effects and heat addition to the gas, the gas behaves in an isentropic way. This is an end-member case that considers a frictionless gas. The effects of isentropic expansion on the slug pressure and volume are governed by the following laws:

$$\frac{P_I}{P_F} = \left(\frac{T_I}{T_F}\right)^{\frac{\delta}{\delta-1}} = \left(\frac{D_F}{D_I}\right)^{3\delta} \quad (10)$$

where P_I, T_I, and D_I are the respective slug pressure, temperature, and (spherical) diameter during the final moments of ascent, P_F, T_F, and D_F are the respective slug pressure, temperature, and diameter when bursting occurs, and δ is the ratio of the gas specific heats at constant pressure and constant volume (1.2 for a mix of H_2O and CO_2 at ~1000°C). Considering that the gas was at the lake temperature before the isentropic expansion gives T_I = 1353 K, and assuming that skin rupture brings the gas to atmospheric pressure gives P_F = 0.65 bar. For each explosion, we set T_F to the equilibrium gas temperatures calculated from the FTIR species ratios (Figure 8b), and equation (10) gives P_I and the size ratio D_F/D_I. We call P_I the pre-bursting pressure because it corresponds to the pressure at which the slug was just prior to cooling. This could be when the slug is bulging at the lake surface if the slug is over-pressured, or when the slug is still below the lake surface if its pressure is controlled by the weight of magma above. In the latter case, P_I can be converted into a maximum depth by assuming no bubble overpressure and a magma-static pressure gradient within the lake. Figure 9 shows the pre-bursting pressure, depth, and relative size of each slug during the final moments of ascent. These data show that the lower equilibrium temperatures represented by the gas explosions can be explained by isentropic cooling from <5 bar to atmospheric pressure, when slugs had reached >50% of their final, bursting sizes. Slugs could thus have started isentropic expansion either from the lake surface in an over-pressured state, or from a depth <15 m if no overpressure is assumed.

[32] To what extent does such cooling affect gas chemistry and contributes therefore to the distinct signal that explosions have compared with quiescent degassing? Starting from the equilibrium temperature, we used D-Compress to reheat and recompress the measured gas composition of each explosion

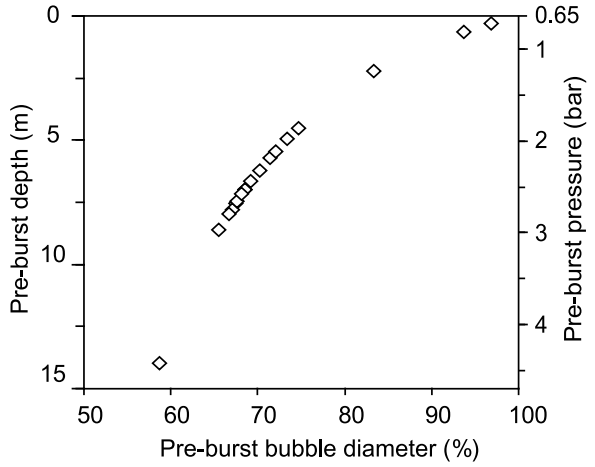

Figure 9. Pressure, maximum depth, and relative size of the gas slugs that generated the 18 explosions measured in December 2005. "Pre-burst" refers to the state just prior the isentropic expansion of the slugs, during their final moments of ascent. Depth conversion assumes slugs reach the surface without overpressure.

back to 1080°C and pre-burst pressures (Figure 9). This yielded the composition of the slugs as they approach the surface but are still at lake temperature, just prior to the isentropic expansion that accompanies bursting. Figure 10 compares the original four measured species ratios to the recalculated values. The ratio of the two dominant species, CO_2/H_2O, is barely affected by the removal of the isentropic expansion (<5%). The three other ratios, in contrast, change appreciably, typically by a factor two and, for SO_2/OCS, by more than 2 orders of magnitude.

[33] Our primary goal is to assess whether the quiescent degassing and the explosions might have a common origin. It is apparent in Figure 10, however, that explosions have pre-burst compositions distinct from that of the effusive gas and thus that the isentropic expansion preceding explosion does not explain the differences between effusive and explosive gas signatures. Recompressing both gas types to higher pressure, however, will change their compositions, possibly defining a common compositional source. We selected three representative gas compositions to simplify the comparison and to conduct further recompressions. For effusive degassing, we used the average gas composition at 1080°C shown in Figure 6. For post-burst explosive data, a median gas composition was obtained by taking the median of the four ratios and calculating an equilibration temperature at atmospheric pressure (829°C). For pre-burst data, we took the medians of the pressures and three ratios (CO_2/CO, CO_2/SO_2, and H_2O/CO_2), and calculated the equilibrium value of SO_2/OCS at 1080°C. These three representative

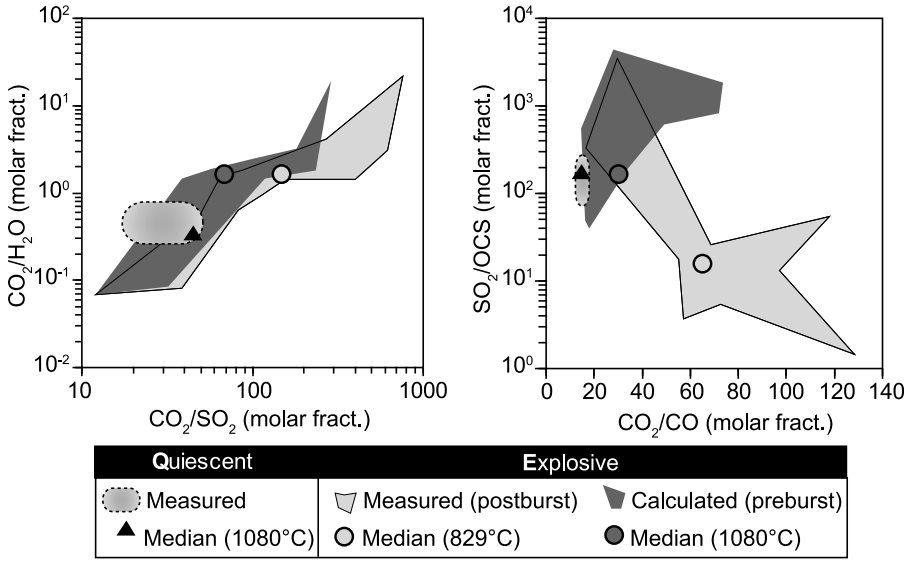

Figure 10. Gas compositions represented by four species ratios. Light gray areas indicate the span of measured pre-burst values of the 18 explosions, with "post-burst" referring to the measured values of the ratios just after slug bursting, when the gas is colder than the lava lake because of isentropic expansion. Dark gray areas with solid line contour indicate the span of pre-burst values of the 18 explosions, with "pre-burst" referring to the calculated values of the ratios before the isentropic expansion of the slugs, during their final moments of ascent. Note the strong effect of gas cooling on composition. Light gray areas with dotted contour indicate the span of values measured during quiescent degassing (cf. Figure 6). The three symbols (dark gray circles, light gray circles, and black triangles) indicate median values for pre-burst, post-burst, and quiescent gas compositions, respectively.

compositions are shown in Figure 10 and Table 1, and are used below to backtrack the degassing process.

5. Backward Tracking of Equilibrium Conditions

[34] The feeding system below Erebus lava lake features a complex circulation pattern able to generate regular lake overturns and fast gas rise that lead to sometimes powerful Strombolian explosions. We frame this rich behavior by carrying out four types of recompression involving more and more complex levels of modeling but all assuming isothermal conditions.

[35] The simplest backtracking is that of the gas only because it simply involves respecting mass balance while maintaining the equilibria stipulated by reactions (1)–(6). Physically, it implies that the gas has no chemical exchange with the melt. For the quiescent degassing, it means that the gas rises independently from the melt, but is in equilibrium with it at all pressures. In other words, gas rises from any point within the magmatic column and only encounters melt that is in equilibrium with it during ascent. This quiescent run thus simulates a "stagnant melt column" undergoing steady degassing. For the explosions, no chemical exchange between gas and melt is expected if the gas rises rapidly as a slug, but it is unlikely if it is rising slowly or is composed of a bubble swarm (see below). Visual observations support explosions being caused by large bubbles breaking the lake surface, which drives us to refer to this run as "fast slug."

[36] Recompression of the median quiescent gas and of the pre-burst median gas (Table 1) yielded the evolution of the four gas ratios as a function of pressure (Figure 11). The CO_2/CO and CO_2/H_2O ratios are the most reliable because the SO_2 content deduced from the field measurements by FTIR spectroscopy might include some or all sulphur from the absent H_2S (see Methods). The SO_2/OCS ratio, on the other hand, is the least reliable one because the equation of state for OCS is valid up to 400 bars, whereas our simulations reach 3000 bars. We thus framed the possible behavior of OCS at higher pressure by carrying out two extrapolations of OCS density. Inspection of Figure 11 shows that common values are reached by the explosive and quiescent backtrackings for CO_2/SO_2 and SO_2/OCS but not for the two other ratios. This would suggest the absence of a common gas source for these two scenarios, but stagnant melt column and fast gas slugs are only open-system end-members. Considering the two respective counterpart scenarios in closed system, a convecting melt column and slow gas slugs, is thus necessary to frame the possible range of degassing behavior.

[37] Closed-system backtracking involves respecting mass balance while maintaining the equilibria stipulated by reactions (1)–(7) and by the solubility laws for H_2O, SO_2, H_2S, H_2, and CO_2. Physically, it implies that the gas is in equilibrium with the surrounding melt at all times. In addition to initial gas composition, this backtracking also requires an initial gas fraction, or porosity. For quiescent degassing, we assume that gas and melt rise together in closed system to reach 40 vol.% porosity at the surface. Closed system rise is supported by visual observation of the upwellings within the lake, which have been linked to convective motions within the shallow plumbing system feeding the lake [*Oppenheimer et al.*, 2009]. The value of 40 vol.% is meant to represent a lake surface porous enough to ensure permeable gas flow [*Burgisser and Gardner*, 2004]. Should a much higher initial porosity be assumed, say >90 vol.%, the resulting run would resemble that with gas only in Figure 11 (see *Burgisser et al.* [2008] for more details). Below 60 vol.%, the evolution of the chemical composition is not very sensitive to the value of porosity assumed at the surface. This can be illustrated by the maximum changes in gas ratios between runs starting from three different initial porosities. Taking the 40 vol.% run as a reference, CO_2/SO_2, CO_2/CO, CO_2/H_2O, and SO_2/OCS change by at most 130%, 0.5%, 110%, and 90%, respectively, when either increasing initial porosity to 60 vol.%, or decreasing it to 10 vol.%. These amounts are roughly twice those related to model uncertainties. The 40 vol.% run will be referenced to as simulating a "convecting magma column." For explosions, we assume that gas and melt rise together in closed system to reach 90 vol.% porosity at the surface. The 90 vol.% porosity value was chosen so as to represent a slug with a thin entrained melt shell. Like in the quiescent case, should a much thinner shell and a higher porosity be assumed for the closed system, say 99 vol.%, the resulting run would resemble that with gas only. An arbitrary value of 90 vol.% thus represents a slug moving slowly enough to maintain chemical equilibrium with a thin melt shell until it reaches the surface. This scenario assumes a small enough rising velocity for the gas phase but only calculates a gas/melt ratio. The gas can thus be envisioned either as a growing single slug with its thin melt shell or as a swarm of small bubbles that undergo coalescence until forming the observed

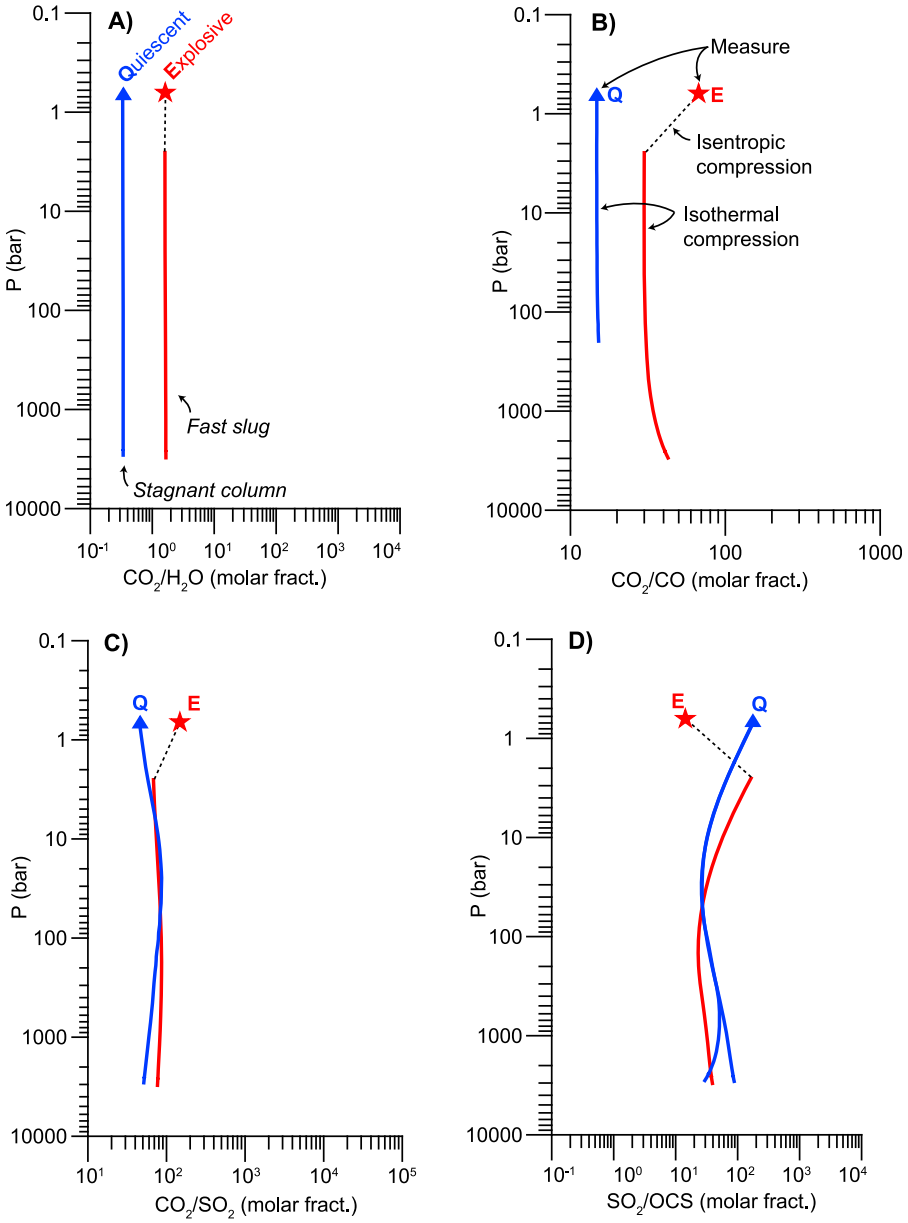

Figure 11. Evolution of the gas composition as a function of pressure. Blue triangles represent the gas measured at the quiescent lake surface and red stars represent the median explosive gas composition. Blue curves represent backtracking of a stagnant column and red curves represent backtracking of fast slugs. Black dotted lines link the measured post-burst compositions to higher pressure, pre-burst values assumed to equilibrate at the quiescent lake temperature of 1080°C. Model uncertainties are smaller than curve thickness. (a) CO_2/H_2O ratio. (b) CO_2/CO ratio. (c) CO_2/SO_2 ratio. (d) SO_2/OCS ratio. Two runs have been carried out for this ratio, each with a different γ factors for OCS. The run with the lower SO_2/OCS has a constant γ above 400 bars, the other not (see text).

large bubble at the lake surface. For simplicity, we refer to this run as simulating a "slow slug."

[38] Figure 12 summarizes the behavior of the four gas ratios as a function of pressure for the four end-member runs. Starting from the quiescent gas composition at atmospheric pressure, there are two possible evolutions, one for the convecting column and the other for the stagnant column. Numerical simulations of the magmatic system of Erebus suggest that complex convection patterns are likely, with convection cells occurring at various levels within the conduit [*Molina et al.*, 2012]. The magma column may thus have any volatile composition between these two runs (light gray areas in Figure 12). Starting from the pre-burst explosive gas composition, there are two possible evolutions, one for the

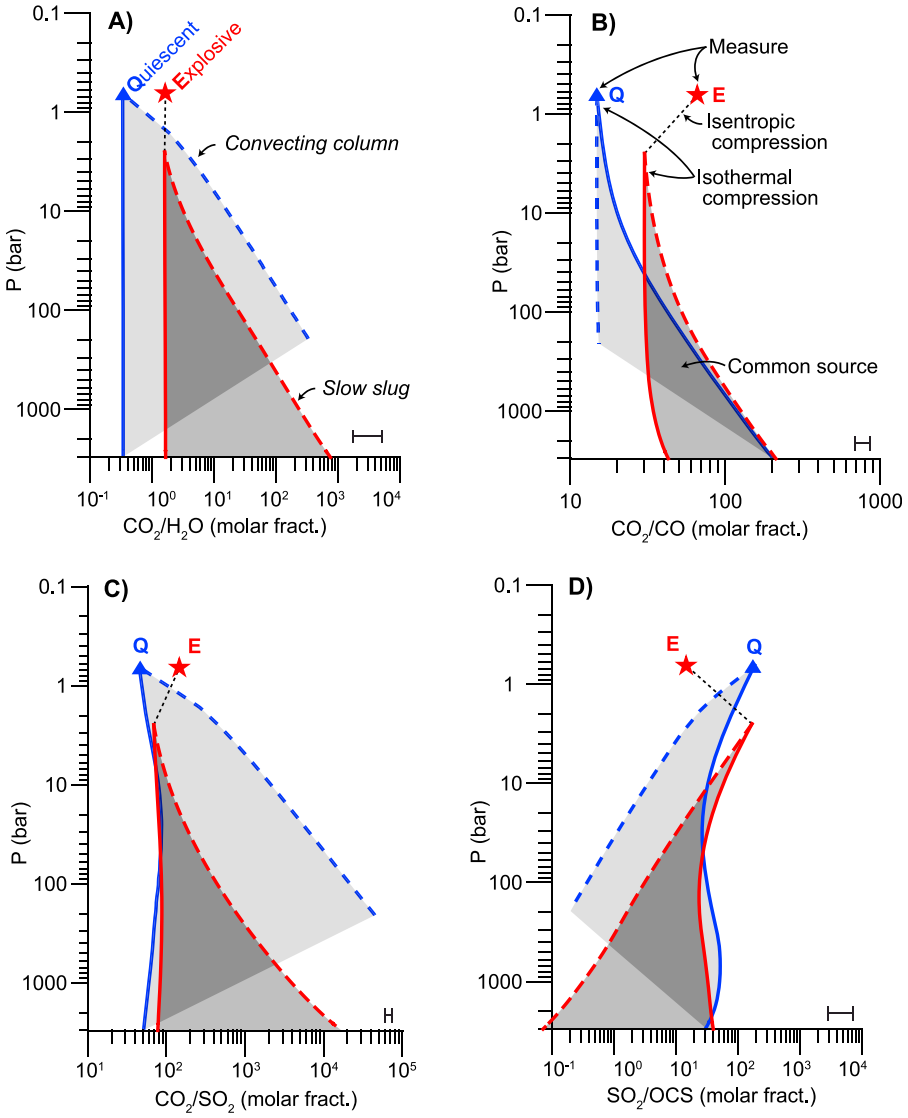

Figure 12. Evolution of the gas composition as a function of pressure. Blue triangles represent the gas measured at the quiescent lake surface and red stars represent the median explosive gas composition. Blue curves represent backtracking of a convecting (dashed curve) and stagnant (solid curve) column and red curves represent backtracking of slow (dashed curve) and fast (solid curve) slugs. Solid curves are identical to those of Figure 11, except that the SO_2/OCS run with a variable γ above 400 bars was discarded for clarity. Black dotted lines link the measured post-burst compositions to higher pressure, pre-burst values assumed to equilibrate at 1080°C. Grey areas cover the span of model outputs for quiescent (light gray) and explosive (medium gray) degassing, with the dark gray area marking the overlap (common source) between these two fields. Horizontal error bars represent the model uncertainties for the closed system runs (dashed curves), and model uncertainties for open system runs (solid curves) are smaller than curve thickness.

slow slug scenario and the other for the fast slug scenario. The various explosion magnitudes observed [*Gerst et al.*, 2008; *Johnson et al.*, 2008] suggest that slugs have variable sizes (and thus rising speeds) in the conduit. As a result, slugs may have any composition between the fast and slow end-member values (medium gray areas in Figure 12). Any magma parcel rising from the region delimited by the overlap of the quiescent and explosive fields can produce either a quiescent degassing signature, or an explosive signature, depending on rise conditions. This overlap region (dark gray areas in Figure 12) defines the sought common source.

[39] Overall, the resulting common fields of values of Figure 12 correspond to a pressure domain >40 bars and indicate that some end-members are more likely than others. Recompression of two additional gas compositions that represent the full span of measured gas ratios extends this conclusion by showing

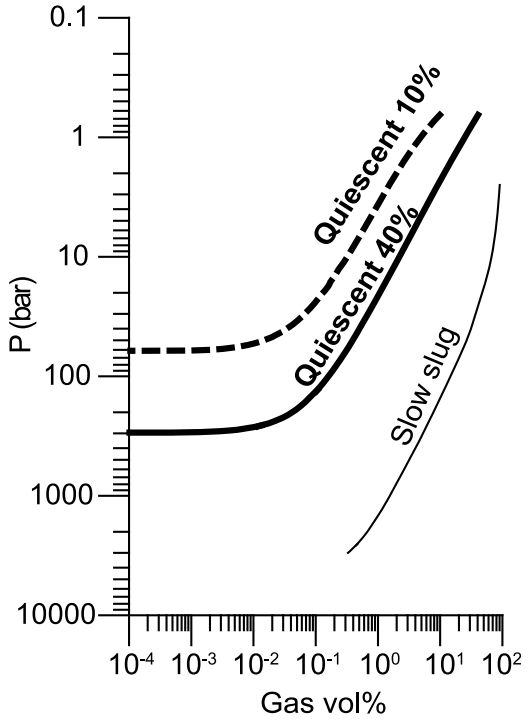

Figure 13. Evolution of gas volume fraction, or porosity, as a function of pressure. Runs labeled "quiescent" started from the same median gas composition measured during passive degassing of the lava lake, but with different porosities at the surface (10 and 40 vol%). The run labeled "slug" started from the median explosive gas composition and 90 vol% porosity.

that the common source of some explosions can be as shallow as 20 bars, a value that we will keep hereafter (Figure S1 in Text S1 in the auxiliary material). It is apparent in Figure 12 that three ratios (CO_2/CO, CO_2/SO_2, and SO_2/OCS) point to a mostly stagnant magmatic column because the convecting end-member often lies outside the common fields. In the context of the long-lived, convecting lava lake at Erebus, a mostly stagnant magmatic column means that the gas phase tends to rise through the system faster than the melt, equilibrating with it over the whole height of the magmatic column. Slow slug rise at depth is strongly suggested by the behavior of CO_2/H_2O because it does not change when slugs rise fast. In other words, the observed variation of CO_2/H_2O can only be explained if there are volatile exchanges between gas and melt. It is likely, however, that a transition between slow and fast ascent occurs at low pressure (maybe a few tens of bars) because of slug acceleration. We interpret the array of explosive compositions as being caused by large bubbles or bubble swarms that originate from various depths in the system, entraining the surrounding melt and rising with it until being left behind by slug acceleration. This entrained melt provides volatiles to the slug or bubble swarm, modifying the gas composition of the rising gas/melt batch compared to the gas generated by quiescent degassing. Although our model does not address slug creation, one likely hypothesis is that slugs originate from horizons where bubble accumulation and coalescence is promoted [e.g., *Jaupart and Vergniolle*, 1989; *Thomas et al.*, 1993; *Menand and Phillips*, 2007].

[40] There are lower pressure bounds for the two closed-system scenarios (convecting column and slow slug) because an initial gas volume fraction has to be assumed for the surface measurement (Figure 12). Figure 13 shows the evolution of gas volume fraction with pressure for the quiescent and the explosive situation. Slugs reaching 90 vol% porosity at the lake surface can originate from >3000 bars, outside of the validity domain of the model. No specific constraint can thus be set by this run. A pressure bound within the validity of the model, however, is clearly visible for the quiescent runs. Would magma rise from greater depths, its porosity at the surface would exceed the assumed starting porosity. It implies that convection can only affect the upper 60 or 300 bars of the conduit if the convecting lava reaches 10 or 40 vol% porosity at the lake surface, respectively. The value of 10 vol% porosity is arbitrary but nicely illustrates the dependence of the maximum pressure on the assumed total volatile content. Our results thus suggest explosive gases are due to slugs rising from at least 20 bars but at most a few hundred bars because the magmatic column feeding the quiescent regime is closer to the stagnant end-member than the convecting end-member.

5.1. Assessment of Some Critical Modeling Assumptions

[41] We quantify in this section the effects of three assumptions related to closed system degassing. Closed-system scenarios (convecting column and slow slug) involve, by definition, dissolved volatile species. All runs presented so far are iron buffered, which means that the oxygen locked or released by the dissolved iron affects the redox state. The relationship used by the thermodynamical model is calibrated with sulphur-free melts and its relevance to the present situation is subject to caution. To quantify the effect of the dissolved iron on the redox state, we compared the evolution of the redox state with pressure when buffering of the oxygen fugacity is

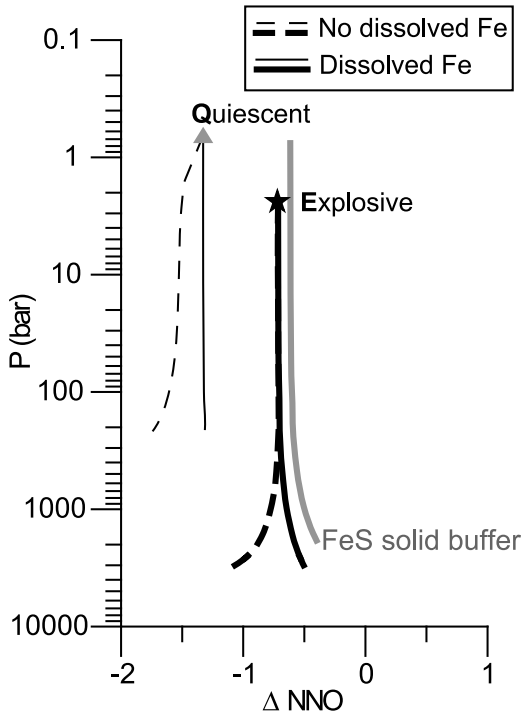

Figure 14. Evolution of the redox state as a function of pressure. The triangle represents the quiescent gas composition and the star represents the median explosive gas composition. Quiescent runs correspond to a convecting column and explosive runs are slow slugs. Solid lines are runs buffered by 5 wt% total FeO, and dashed lines are runs buffered by the gas phase only. The redox state at which FeS saturation occurs at 1000°C is also shown.

controlled by either the gas phase, or the dissolved Fe (Figure 14). As expected, iron helps in maintaining a constant redox state in the convecting magma column feeding the quiescent degassing. Without its effect, the fO_2 in the column would be about 0.3 log units lower. A similar reducing effect occurs above 1000 bars for slow slugs. Translated into changes in gas ratios, these reducing effects lower CO_2/CO by <50%, SO_2/OCS by <70%, CO_2/SO_2 by <40%, and CO_2/H_2O by ≪1%. Overall, iron buffering affects gas ratios to a degree comparable to model uncertainties and has far less impact on model outputs than whether degassing occurs in closed or open system.

[42] A likely mineral buffer at Erebus is FeS, when saturated. Model runs presented in *Oppenheimer et al.* [2011] take this buffer into account, whereas our runs do not. Following the work of *Moretti and Baker* [2008], the redox state at which FeS saturation occurs at 1000°C is indicated in Figure 14. This buffer is almost constant at NNO–0.6 and parallels the evolution of slugs. It is, however, at odds with the equilibrium redox state of the quiescent gas, and would correspond to that of a stagnant magma column at 60 bars (compare Figures 11 and 14). Taking FeS saturation into account in our model would thus mostly affect the backtracking of the quiescent gas but would require an additional mechanism to oxidize the gas from its atmospheric value to that of FeS saturation.

[43] All our calculations are conducted at thermodynamic equilibrium. What would be the effects of a partial kinetic disequilibrium between gas and melt, if a few species only were not diffusing fast enough into the bubbles while the others kept pace? Of all soluble species considered in our modeling, sulphur-bearing ones are the most likely affected by kinetics owing to their low diffusivity [*Baker et al.*, 2005]. We suppressed S exchange between gas and melt by assuming that S is insoluble (i.e., the S initially present in the gas remains gaseous and the S present in the melt remains dissolved during recompression). Resulting runs suggest that, overall, sulphur degassing mostly affects S-bearing ratios (CO_2/SO_2 and SO_2/OCS) and that partial kinetic disequilibrium between gas and melt causes model outputs to resemble gas-only runs, where all gas species are out of equilibrium with the surrounding melt. This is illustrated by Figure 15, which shows the evolution of CO_2/SO_2 with pressure for a melt that degases all soluble species but sulphur. Without S degassing, the run representing the convecting magma column remains constant (like a stagnant column) from the surface to 200 bars, above which there is a sharp decrease of CO_2/SO_2. A similar behavior occurs in the explosive regime, where the absence of S degassing causes slow-rising slugs to maintain an almost constant CO_2/SO_2 of 100 over the whole recompression, much like fast-rising slugs do (compare Figures 11 and 15). Anomalies of kinetic nature have timescales comparable with the frequency of measurement (1 Hz), as long as other uncertainties such as atmospheric conditions can be discarded. These measurements indicate a remarkable steadiness of the quiescent gas composition (Figure 1), which drives us to consider that this regime is unaffected by slow diffusion of dissolved volatiles. Slugs driving the explosions, on the other hand, might be affected by diffusion kinetics; large and fast slugs being better candidates than slow slugs or bubble swarms. Taking into account kinetic effects at Erebus would thus leave our equilibrium

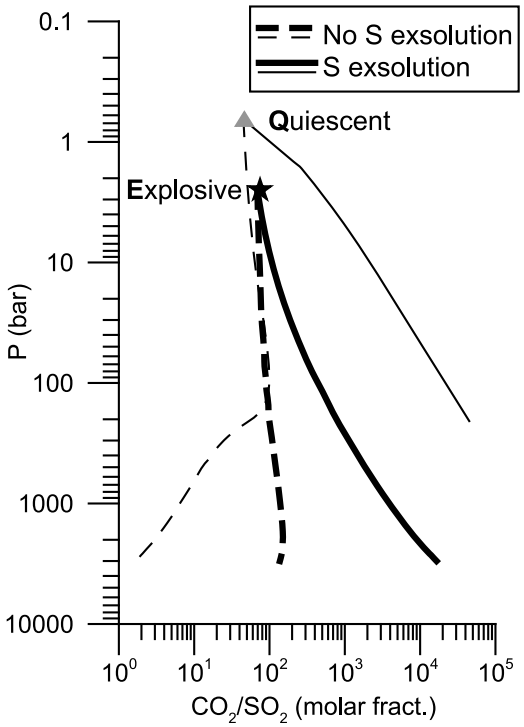

Figure 15. Evolution of CO_2/SO_2 as a function of pressure. The triangle represents the quiescent gas composition and the star represents the median explosive gas composition. Quiescent runs correspond to a convecting column and explosive runs are slow slugs. Solid lines are runs allowing S to degas in equilibrium, and dashed lines are runs that assume no S exchange between the gas and the melt.

runs for the quiescent regime unchanged but bring the explosive runs toward the "fast slug" end-member.

6. Discussion

[44] Values of 1069–1084°C for the equilibrium composition of the quiescent gas most likely reflect the lake temperature. It is, however, higher than that quoted in the literature (980–1030°C) [*Kyle*, 1977; *Dunbar et al.*, 1994]. The previously reported figures were based on mineral geothermometry, melt inclusion homogenization temperatures and optical pyrometer readings made on a bursting bubble. The range of values given by these various methods is not surprising as the gas is emitted from a convecting lake with temperature gradients caused by processes such as recycling of chilled crust and feeding from warm upwellings. The pyrometer measurements were uncorrected for emissivity (which would lead to underestimation of the thermodynamic temperature) but more significantly the rapid formation of a cooler skin on fiercely radiating incandescent lava will inevitably result in underestimation of magma temperature by either thermography or pyrometry. We have also applied the widely used *Harrison and Watson* [1984] apatite geothermometer taking the matrix glass SiO_2 and P_2O_5 content reported for 29 samples of Erebus phonolite in *Kelly et al.* [2008], which suggest a temperature of $\sim$1110 $\pm$ 20°C. Notwithstanding the high F content of Erebus apatite (3 wt.%) that may affect this geothermometer, this value is much closer to the results of our gas geothermometry. Although discrepancies between methods that do not characterize the same objects (melt + crystals and melt + gas, respectively) are expected, they drove us to test other aspects regarding the assumed thermodynamical equilibrium of the quiescent gas.

[45] At ΔNNO = $-$1.33 (the median quiescent redox state, Table 1), our model indicates that the molar ratio of H_2S/SO_2 should be 1.2 at 1000°C and 0.2 at 1080°C. Regardless of temperature, these ratios amount to a quantity of H_2S that should visibly affect the IR spectra. The lack of H_2S detection by FTIR (see Section 2.2) is an argument against the gas being in equilibrium, but a puzzling one considering the consistency of the time series behavior of the other measured species and the reducing conditions of the lava lake. Besides instrumental bias, one possibility is that atmospheric reactions are removing H_2S [*Martin et al.*, 2009]. Assuming that all H_2S is being combusted to SO_2 by atmospheric oxygen changes the calculated gas molar fractions (Table S3 in Text S1 in the auxiliary material) by less than 1%, which has negligible impact on SO_2/OCS or our gas geothermometry. The equilibrium calculations thus seem robust against such atmospheric process. Another argument in favor of equilibrium comes from a series of measurements with the "MultiGas" instrument [*Moussallam et al.*, 2012]. It yielded H_2/SO_2 values $\sim$1–2 for a period of quiescent degassing at the end of 2010, which is comparable to (although lower than) the ratios predicted by our model for the end of 2005 (between 2.2 and 4.6, Table S3 in Text S1 in the auxiliary material). Yearly and instrumental differences remain to be assessed in detail, but it is noteworthy that CO_2/SO_2 values overlap: 36–45 in 2010 and 20–45 in 2005.

[46] An important result is that a significant part of the explosive signature is inherited during gas cooling at very shallow pressure. Isentropic recompression yields slug overpressures up to 4.5 bars, which fit nicely with the independent estimates of 1 to 6 bars done by A. Gerst et al. (The first second of a Strombolian volcanic eruption: Energies, pressures, mechanisms, submitted to *Journal of*

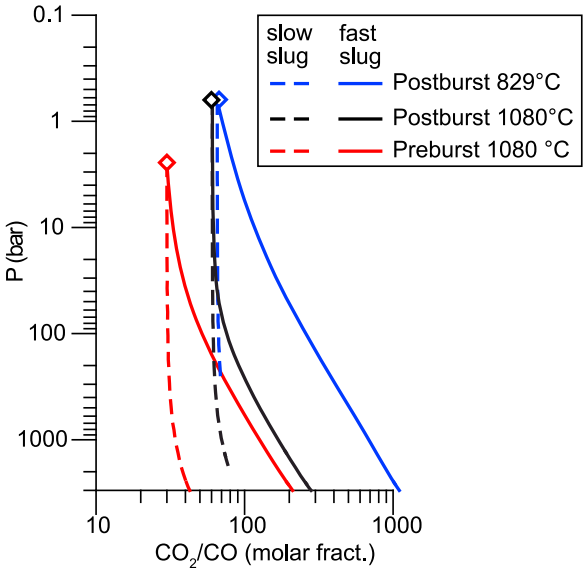

Figure 16. Evolution of CO_2/CO as a function of pressure for pre- and post-burst gas compositions. Diamonds represent three possible median compositions of the explosive gas from which isothermal backtracking is carried out. Solid and dotted lines represent fast and slow slugs, respectively.

Geophysical Research, 2012). Can one, however, overlook the isentropic cooling of the slugs just prior to bursting, like it has been done at Stromboli, for instance [*Burton et al.*, 2007]? Figure 16 shows pairs of compression runs (slow and fast slugs) for three possible starting gas compositions. The first pair of runs starts, for reference, from the pre-burst composition at 2.5 bars and reheated to 1080°C. The two other pairs are uncorrected for cooling. The second pair starts with a gas at 829°C and 0.65 bar composed of the respective median values of the four chemical ratios listed in Table 1. The third pair starts with a gas at 0.65 bar composed of the respective median values of only three ratios (CO_2/H_2O, CO_2/CO, and CO_2/SO_2). Cooling is ignored in this run by assuming an equilibrium temperature of 1080°C, which implies that SO_2/OCS is overestimated (Table 1). Figure 16 shows that slow slugs (i.e., closed-system degassing) have a nearly constant CO_2/CO over the range of pressures considered. Ignoring isentropic cooling would thus yield a global CO_2/CO over-estimation, which corresponds to over-estimating the magma column redox state. Fast slugs (i.e., gas-only compression) have a different behavior. Their CO_2/CO ratios increase in variable proportions at pressures higher than 100 bars. The increase is less marked when the gas is initially close to the NNO buffer, like it is the case for the uncorrected slug (Table 1). Correcting for the isentropic cooling of the slugs has thus significant consequences on the backward tracking results.

[47] The continuous degassing at Erebus sheds an interesting light on what may control oxygen fugacity during magma ascent. If buffering of the oxygen fugacity is assumed to be controlled by mineral species, such as in *Oppenheimer et al.* [2011], changes are expected to be more sluggish than ascent rates, and might occur deeper in the magmatic system. The mineral-buffered redox simulations by *Oppenheimer et al.* [2011] yield two deep sources linked to quiescence (phonolite, ~1–3 kbar) and explosions (basanite, ~5–8 kbar), respectively, with various degrees and depth of mixing between the magma types. Assuming, as we do here, that the gas phase controls redox trends causes a shallower and simpler picture to emerge. We studied four degassing scenarios that involve various degrees of separation between gas and melt, but that do not necessitate mixing of distinct magma batches. Our simulations suggest the possible existence of a single phonolitic source >20 bars for quiescent and explosive gases. Gas-buffered redox changes are expected to operate on timescales faster than tens of seconds, which readily explains why CO_2/CO ratio variations are in phase with the shallow pulsatory degassing of the lake (Figure 7). Differences in oxidation state between quiescent and explosive gas are partly due to pre-burst cooling (Table 1) and partly due to the redox change within the plumbing system (illustrated as changes in CO_2/CO in Figure 12). The single magmatic source is also consistent with the mineral chemistry of the phonolite in the lava lake, which indicates NNO–1.8 at 1000°C [*Kelly et al.*, 2008], and with calculations based on sulphide content at sulphur saturation for anorthoclase-hosted melt inclusions in the phonolite, which record conditions close to NNO–0.5 (Figure 14) [*Oppenheimer et al.*, 2011]. These redox states correspond to respective CO_2/CO values of 13 and 50, within the span of backtracked quiescent gas compositions above 200 bars (Figure 12). In our view, discrimination between redox control by the gas phase (this work) versus redox control by the melt and crystalline phases [*Oppenheimer et al.*, 2011] could most easily achieved by direct temperature measurements of the lake. Such contrasting characterizations of persistent sources of volatiles from which Strombolian explosions arise at Erebus reflect the level of understanding we have achieved so far in relating gas chemistry to deeper magmatic processes. The way forward, in our view, is to integrate into the various approaches the widely different timescales over

which bubble rise, melt migration, and crystallization control the oxidation state of magmas.

7. Conclusions

[48] We used the molecular composition of the gas discharged from the phonolite lava lake in the summit crater of Erebus volcano, Antarctica, to infer the subsurface behavior of the magma. Chemistry was determined from infrared absorption spectra that yielded the ratios (CO_2/CO, CO_2/H_2O, CO_2/SO_2, and SO_2/OCS) of five gas species. This chemistry was interpreted thanks to the thermodynamic model D-Compress [*Burgisser et al.*, 2008], which is based on gas buffering of the redox state, and which we calibrated for phonolitic melts.

[49] During quiescent degassing of the lava lake, the gas composition calculated at thermodynamic equilibrium and atmospheric pressure suggests that the lake temperature is ~1080°C and $f\,O_2$ is about 0.5 log units below the QFM buffer at this temperature (ΔNNO = −1.33). Strombolian explosions that episodically disturb the lake surface have species ratios that are quite distinct from the quiescent degassing values. The explosion gases most likely reflect equilibration temperatures at 0.65 bar ranging from 700 to 1050°C. These colder temperatures are the result of closed-system depressurization of the gas along an isentropic adiabat from pressures <5 bar down to the local atmospheric pressure, when gas slugs are at more than 50% of their final, bursting sizes. The ratio of the two dominant species, CO_2 and H_2O, is barely affected by the isentropic expansion (<5%). The three other ratios change appreciably, typically by a factor two and sometimes by more than two orders of magnitude. The isentropic cooling of the slugs just prior to bursting has thus a major effect on gas composition and affects model outcomes when taken into account.

[50] We performed backward tracking of the gas data using the same thermodynamic model. We carried out two isothermal recompression runs from atmospheric pressure to 3 kbar of the quiescent gas composition emitted through the lake. The first run assumes that gas and melt rise together in closed system to reach a given porosity at the surface, which corresponds to an actively convecting magma column. The second run assumes that the gas is rising independently from the melt, which corresponds to the passive, open-system degassing of a stagnant magma column. We used these two end-member runs as the quiescent volatile field of reference by considering that the magma column may have any volatile composition in between. Our results imply that convection can only affect the upper 60 or 300 bars of the conduit if the convecting lava reaches 10 or 40 vol% porosity at the lake surface, respectively.

[51] We carried out two reference runs by isothermal recompression of the pre-burst, explosive gas composition. The first run assumes a gas slug or bubble swarm moving slowly enough to maintain chemical equilibrium with a thin melt shell and the second run assumes that the slug is rising rapidly without any chemical exchange with the melt. Each run predicts a distinct evolution of the four species ratios with increasing pressure. There again, any value between the two runs is deemed possible, which defines a field of values from which explosive gases originate. The observed overlap between the quiescent and the explosive fields means that it is possible to generate both quiescent and explosive gas signatures from a single phonolitic magma batch rising according to the respective degassing scenarios. This overlap and the evolution of three ratios (CO_2/CO, CO_2/SO_2, and SO_2/OCS) point to a mostly stagnant magmatic column generating the quiescent gas signature. All four ratios suggest explosive gases are due to slugs rising from at least 20 bars but at most a few hundred bars because the magmatic column feeding the quiescent regime is closer to the stagnant end-member than the convecting end-member. Slow slug rise at depth is strongly suggested by the behavior of CO_2/H_2O because its variations can only be explained if there are volatile exchanges between gas and melt. Differences between explosions can be due to various departure depths and/or slug acceleration below a few tens of bars.

[52] We evaluated the impacts of two critical assumptions of the model. The first is that our treatment of the buffering effect of iron dissolved in the melt does not account for the effect of other dissolved volatiles such as sulphur. Runs with and without iron buffering suggest it mostly affects $f\,O_2$ and CO_2/CO and has less impact on model outputs than whether degassing occurs in closed or open system. The second assumption is that degassing occurs in equilibrium. Kinetic disequilibrium between gas and melt causes model outputs to resemble gas-only runs. Restricting sulphur degassing because it is the slowest diffusing species mostly affects S-bearing ratios (CO_2/SO_2 and SO_2/OCS). None of these assumptions change the main conclusion of our work, which is that differences between quiescent and explosive gas signatures can be explained by the individual rise of gas and melt batches from a single, potentially very shallow, phonolitic source.

Acknowledgments

[53] We thank G. Iacono Marziano for her help to interpret the CO_2 data from her PhD thesis and R. Moretti for an in-depth review of an earlier version of this manuscript. We also thank D. Baker and J. Lowenstern for their constructive reviews and J. Tyburczy for his editorial help. This research was supported by grants ANT- 0838817 from the Office of Polar Programs (National Science Foundation), 202844 from the European Research Council (under the European FP7), and Le Studium® Institute of Advanced Studies.

References

Aster, R., D. Zandomeneghi, S. Mah, S. McNamara, D. B. Henderson, H. Knox, and K. Jones (2008), Moment tensor inversion of very long period seismic signals from Strombolian eruptions of Erebus volcano, *J. Volcanol. Geotherm. Res.*, *177*, 635–647, doi:10.1016/j.jvolgeores.2008.08.013.

Baker, D., and R. Moretti (2011), Modeling the solubility of sulfur in magmas: A 50-year old geochemical challenge, *Rev. Mineral. Geochem.*, *73*, 167–213, doi:10.2138/rmg.2011.73.7.

Baker, D. R., C. Freda, R. A. Brooker, and P. Scarlato (2005), Volatile diffusion in silicate melts and its effects on melt inclusions, *Ann. Geophys.*, *48*, 699–717.

Boichu, M., C. Oppenheimer, V. Tsanev, and P. R. Kyle (2010), High temporal resolution SO_2 flux measurements at Erebus volcano, Antarctica, *J. Volcanol. Geotherm. Res.*, *190*, 325–336, doi:10.1016/j.jvolgeores.2009.11.020.

Boichu, M., C. Oppenheimer, T. J. Roberts, V. Tsanev, and P. Kyle (2011), On bromine, nitrogen oxides and ozone depletion in the tropospheric plume of Erebus volcano (Antarctica), *Atmos. Environ.*, *45*, 3856–3866, doi:10.1016/j.atmosenv.2011.03.027.

Burgisser, A., and J. E. Gardner (2004), Experimental constraints on degassing and permeability in volcanic conduit flow, *Bull. Volcanol.*, *67*, 42–56, doi:10.1007/s00445-004-0359-5.

Burgisser, A., and B. Scaillet (2007), Redox evolution of a degassing magma rising to the surface, *Nature*, *445*, 194–197, doi:10.1038/nature05509.

Burgisser, A., B. Scaillet, and Harshvardhan (2008), Chemical patterns of erupting silicic magmas and their influence on the amount of degassing during ascent, *J. Geophys. Res.*, *113*, B12204, doi:10.1029/2008JB005680.

Burnham, C. W., J. R. Holloway, and N. F. Davis (1969), Thermodynamic properties of water to 1000°C and 10000 bars, *Spec. Pap. Geol. Soc. Am.*, *132*, 96 pp.

Burton, M. R., C. Oppenheimer, L. A. Horrocks, and P. W. Francis (2000), Remote sensing of CO_2 and H_2O emission rates from Masaya volcano, Nicaragua, *Geology*, *28*, 915–918, doi:10.1130/0091-7613(2000)28<915:RSOCAH>2.0.CO;2.

Burton, M., P. Allard, F. Muré, and A. La Spina (2007), Magmatic gas composition reveals the source depth of slug-driven Strombolian explosive activity, *Science*, *317*(5835), 227–230, doi:10.1126/science.1141900.

Carmichael, I. S. E., and M. S. Ghiorso (1986), Oxidation-reduction relations in basic magma: A case for homogeneous equilibria, *Earth Planet. Sci. Lett.*, *78*, 200–210, doi:10.1016/0012-821X(86)90061-0.

De Lauro, E., S. De Martino, M. Falanga, and M. Palo (2009), Decomposition of high-frequency seismic wavefield of the Strombolian-like explosions at Erebus volcano by independent component analysis, *Geophys. J. Int.*, *177*, 1399–1406, doi:10.1111/j.1365-246X.2009.04157.x.

Dibble, R. R., P. R. Kyle, and C. A. Rowe (2008), Video and seismic observations of Strombolian eruptions at Erebus volcano, Antarctica, *J. Volcanol. Geotherm. Res.*, *177*, 619–634, doi:10.1016/j.jvolgeores.2008.07.020.

Dunbar, N. W., K. V. Cashman, and R. Dupré (1994), Crystallization processes of anorthoclase phenocrysts in the Mount Erebus magmatic system: Evidence from crystal composition, crystal size distributions, and volatile contents of melt inclusions, in *Volcanological and Environmental Studies of Mount Erebus, Antarctica*, *Antarct. Res. Ser.*, vol. 66, edited by P. R. Kyle, pp. 129–146, AGU, Washington, D. C.

Gerst, A., M. Hort, P. R. Kyle, and M. Vöge (2008), 4D velocity of Strombolian eruptions and man-made explosions derived from multiple Doppler radar instruments, *J. Volcanol. Geotherm. Res.*, *177*, 648–660, doi:10.1016/j.jvolgeores.2008.05.022.

Giggenbach, W. F. (1996), Chemical composition of volcanic gases, in *Monitoring and Mitigation of Volcano Hazards*, edited by R. Scarpa and R. I. Tilling, pp. 221–256, Springer, Berlin, doi:10.1007/978-3-642-80087-0_7.

Giggenbach, W. F., P. R. Kyle, and G. Lyon (1973), Present volcanic activity on Mt. Erebus, Ross Island, Antarctica, *Geology*, *1*, 135–136, doi:10.1130/0091-7613(1973)1<135:PVAOME>2.0.CO;2.

Harris, A. J. L., R. Carniel, and J. Jones (2005), Identification of variable convective regimes at Erta Ale lava lake, *J. Volcanol. Geotherm. Res.*, *142*, 207–223, doi:10.1016/j.jvolgeores.2004.11.011.

Harrison, T. M., and E. B. Watson (1984), The behavior of apatite during crustal anatexis: Equilibrium and kinetic considerations, *Geochim. Cosmochim. Acta*, *48*, 1467–1477, doi:10.1016/0016-7037(84)90403-4.

Iacono Marziano, G. (2005), Equilibrium and disequilibrium degassing of a phonolitic melt simulated by decompression experiments, PhD thesis. Univ. Palermo, Palermo, Italy.

Ihmels, E. C., and J. Gmehling (2001), Densities of toluene, carbon dioxide, carbonyl sulfide, and hydrogen sulfide over a wide temperature and pressure range in the sub- and supercritical state, *Ind. Eng. Chem. Res.*, *40*, 4470–4477, doi:10.1021/ie001135g.

Jaupart, C., and S. Vergniolle (1989), The generation and collapse of a foam layer at the roof of a basaltic magma chamber, *J. Fluid Mech.*, *203*, 347–380, doi:10.1017/S0022112089001497.

Johnson, J., R. Aster, K. R. Jones, P. Kyle, and B. McIntosh (2008), Acoustic source characterization of impulsive Strombolian eruptions from the Mount Erebus lava lake, *J. Volcanol. Geotherm. Res.*, *177*, 673–686, doi:10.1016/j.jvolgeores.2008.06.028.

Kelly, P. J., P. R. Kyle, N. W. Dunbar, and K. W. W. Sims (2008), Geochemistry and mineralogy of the phonolite lava lake, Erebus volcano, Antarctica: 1972–2004 and comparison with older lavas, *J. Volcanol. Geotherm. Res.*, *177*, 589–605, doi:10.1016/j.jvolgeores.2007.11.025.

Kyle, P. R. (1977), Mineralogy and glass chemistry of volcanic ejecta from Mt. Erebus, Antarctica, *N. Z. J. Geol. Geophys.*, *20*, 1123–1146, doi:10.1080/00288306.1977.10420699.

Kyle, P. R., J. A. Moore, and M. F. Thirlwall (1992), Petrologic evolution of anorthoclase phonolite lavas at Mount Erebus, Ross Island, Antarctica, *J. Petrol.*, *33*, 849–875.

Martin, R. S., T. J. Roberts, T. A. Mather, and D. M. Pyle (2009), The implications of H_2S and H_2 kinetic stability in high-T mixtures of magmatic and atmospheric gases

for the production of oxidized trace species (e.g., BrO and NO_x), *Chem. Geol.*, *263*, 143–150, doi:10.1016/j.chemgeo.2008.12.028.

Menand, T., and J. C. Phillips (2007), A note on gas segregation in dykes and sills at high volumetric gas fractions, *J. Volcanol. Geotherm. Res.*, *162*, 185–188, doi:10.1016/j.jvolgeores.2007.03.002.

Molina, I., A. Burgisser, and C. Oppenheimer (2012), Numerical simulations of convection in crystal-bearing magmas: A case study of the magmatic system at Erebus, Antarctica, *J. Geophys. Res.*, *117*, B07209, doi:10.1029/2011JB008760.

Moncrieff, D. H. S. (1999), Sulphur solubility behaviour in evolved magmas: An experimental study, PhD thesis. Univ. of Bristol, Bristol, U. K.

Moretti, R., and D. R. Baker (2008), Modeling of the interplay of fO_2 and fS_2 along the FeS-silicate melt equilibrium, *Chem. Geol.*, *256*, 286–298, doi:10.1016/j.chemgeo.2008.06.055.

Moretti, R., and G. Ottonello (2003), Polymerization and disproportionation of iron and sulfur in silicate melts: Insights from an optical basicity-based approach, *J. Non Cryst. Solids*, *323*, 111–119, doi:10.1016/S0022-3093(03)00297-7.

Moussallam, Y., C. Oppenheimer, A. Aiuppa, G. Giudice, M. Moussallam, and P. Kyle (2012), Hydrogen emissions from Erebus volcano, Antarctica, *Bull. Volcanol.*, in press.

Newman, S., and J. B. Lowenstern (2002), VolatileCalc: A silicate melt-H_2O–CO_2 solution model written in Visual Basic for Excel, *Comput. Geosci.*, *28*, 597–604, doi:10.1016/S0098-3004(01)00081-4.

Oppenheimer, C., and P. R. Kyle (2008), Probing the magma plumbing of Erebus volcano, Antarctica, by open-path FTIR spectroscopy of gas emissions, *J. Volcanol. Geotherm. Res.*, *177*, 743–754, doi:10.1016/j.jvolgeores.2007.08.022.

Oppenheimer, C., A. S. Lomakina, P. R. Kyle, N. G. Kingsbury, and M. Boichu (2009), Pulsatory magma supply to a phonolite lava lake, *Earth Planet. Sci. Lett.*, *284*, 392–398, doi:10.1016/j.epsl.2009.04.043.

Oppenheimer, C., R. Moretti, P. Kyle, A. Eschenbacher, J. Lowenstern, R. Hervig, and N. W. Dunbar (2011), Mantle to surface degassing of alkalic magmas at Erebus volcano, Antarctica, *Earth Planet. Sci. Lett.*, *306*, 261–271, doi:10.1016/j.epsl.2011.04.005.

Papale, P. (1999), Modeling of the solubility of a two-component $H_2O + CO_2$ fluid in silicate liquids, *Am. Mineral.*, *84*, 477–492.

Papale, P., R. Moretti, and D. Barbato (2006), The compositional dependence of the saturation surface of $H_2O + CO_2$ fluids in silicate melts, *Chem. Geol.*, *229*, 78–95, doi:10.1016/j.chemgeo.2006.01.013.

Schmidt, B., and H. Behrens (2008), Water solubility in phonolite melts: Influence of melt composition and temperature, *Chem. Geol.*, *256*, 259–268, doi:10.1016/j.chemgeo.2008.06.043.

Taran, Y. A., J. W. Hedenquist, M. A. Korzhinsky, S. I. Tkachenko, and K. I. Shmulovich (1995), Geochemistry of magmatic gases from Kudryavy volcano, Iturup, Kuril Islands, *Geochim. Cosmochim. Acta*, *59*, 1749–1761, doi:10.1016/0016-7037(95)00079-F.

Thomas, N., S. Tait, and T. Koyaguchi (1993), Mixing of stratified liquids by the motion of gas bubbles: Application to magma mixing, *Earth Planet. Sci. Lett.*, *115*, 161–175, doi:10.1016/0012-821X(93)90220-4.

Witham, F. (2011), Conduit convection, magma mixing, and melt inclusion trends at persistently degassing volcanoes, *Earth Planet. Sci. Lett.*, *301*, 345–352, doi:10.1016/j.epsl.2010.11.017.

Witter, J. B., V. C. Kress, P. Delmelle, and J. Stix (2004), Volatile degassing, petrology, and magma dynamics of the Villarrica lava lake, southern Chile, *J. Volcanol. Geotherm. Res.*, *134*, 303–337, doi:10.1016/j.jvolgeores.2004.03.002.